海洋生物化学大循環モデルの構築

山 中 康 裕

(1)

海洋生物化学大循環モデルの構築

山 中 康 裕

1994 年 12 月 22 日提出

Development of Ocean Biogeochemical General Circulation Model

Yasuhiro Yamanaka *

Doctoral Dissertation sumitted to University of Tokyo

December 22, 1994

*Center for Climate System Research, University of Tokyo, Komaba 4-6-1, Meguro-ku, Tokyo 153, Japan. E-mail: galapen@ccsr.u-tokyo.ac.jp

Abstract

Two types of an ocean biogeochemical general circulation model (B-GCM), which is a general circulation model coupled with simple biogeochemical processes are developed: one takes into account only particulate organic carbon (POC), and the other both POC and dissolved organic carbon (DOC). Two components of DOC, the semi-refractory DOC and the refractory DOC, are considered.

The phosphate distribution is determined by two parameters, the bioproduction efficiency and the exponent of vertical profile of POC flux, for production and consumption of POC. The phosphate distribution can be reproduced only when the vertical profile of POC flux observed by the sediment traps is adopted. The widely used value of the rain ratio (=0.25), a ratio of production rate of calcite against that of POC, should be modified by taking into account the difference in the remineralization depths of POC and calcite. The value of the rain ratio in the real ocean is found to be 0.06~0.08, when the carbonate sedimentation is included.

The role of DOC in the nutrient and carbon cycles is studied. The distributions of chemical tracers are determined mainly by the vertical POC flux and ocean circulation. The vertical and horizontal DOC fluxes only affect the distribution of the chemical tracers above the depth of 400m. Below that depth, only the inert refractory DOC exists. The export production due to POC consistent with the observed distribution of phosphate is estimated to be about 9GtC/yr, whose value is within the estimates based on the observation. The global export production due to DOC at the depth of 100m is about 6Gt/yr, most of which is transported by the convection. However, the downward nutrients and carbon transports below the depth of 400m are almost due to POC.

The reasonable set for the decay time and the production rate of semi-refractory DOC to explain the observation is estimated to be (0.5yr, 27GtC/yr) $\sim$ (1yr, 18GtC/yr). The production and consumption of the refractory DOC in the deep layer is estimated to be well below 10% of the DOC concentration, if any.

The dependency of the distribution of chemical tracers on these parameters is clarified, and the observed distributions of chemical tracers, such as phosphate and oxygen, are well reproduced. The maximum value of the phosphate concentration exists in the northern part of the North Pacific, which coincides with the observation. The DOC distribution in the surface layer shows that the double DOC maximum zone (DDMZ) extends in the east-west direction in the equatorial Pacific. The observed distribution of $\Delta^{14}C$ of DOC and dissolved inorganic carbon (DIC) in the deep North Pacific and the deep North Atlantic are well reproduced.

Acknowledgements

I would like to express my heartfelt thanks to Prof. Nobuo Suginohara for his helpful discussion and continuous encouragements and also his critical reading of the manuscript. I would also like to thank Dr. Eiichi Tajika for his helpful discussion, and encouragements as a coauthor of the papers. Thanks are extended to Prof. Taro Takahashi for his comments and for giving his data to me.

I thank Drs. Ayako Abe-Ouchi, Ryuji Tada, Yutaka Abe, Hodaka Kawahata, Takashi Ohsumi, Naohiko Ohkouchi, Masafumi Murayama, Makoto Okada, Masao Iwai, Hiroyuki Kumagai, Messrs. Naokazu Ahagon, Tomohisa Irino, and the other members of paleoclimate colloquium for their helpful discussions and comments. I also thank the members of the oceanography laboratory, Dr. Kensuke Nakajima, Messrs. Minoru Nakata, Ichiro Ishikawa, Ryo Furue, Mchio Kawamiya, and Hiroyasu Hasumi for their continuous encouragements.

Helpful discussions on marine chemistry and biology with Drs. Mchio Kishi, Masao Ishii, Hisayuki Inoue, Katsumi Hirose, Eiichiro Tanoue, Takeshi Nakatsuka, Shinichiro Noriki, Messrs. Tsuneo Ono, and Takafumi Aramaki are greatly appreciated. Profs. Akimasa Sumi and Mineo Kumazawa gave me their helpful comments and encouragements which I appreciate. All the colleagues in CCSR and Dr. Atsusi Numaguti are also appreciated for their encouragements. I enjoyed discussions with Mr. Hiroyuki Tsujino and Ms. Tomoe Nasuno during my seminar. The software for graphics on SUN Microsystems developed by Drs. Masanori Yasumitsu and Masakazu Tamura was very useful.

I thank my parents for their continuous support over the years.

Numerical calculations were performed by HITAC M-3800 at the Computer Center of the University of Tokyo. Figures were produced by GFD-Dennou Libraries on SUN Microsystems SS2 and IPX.

Contents

Chapter 1

General Introduction

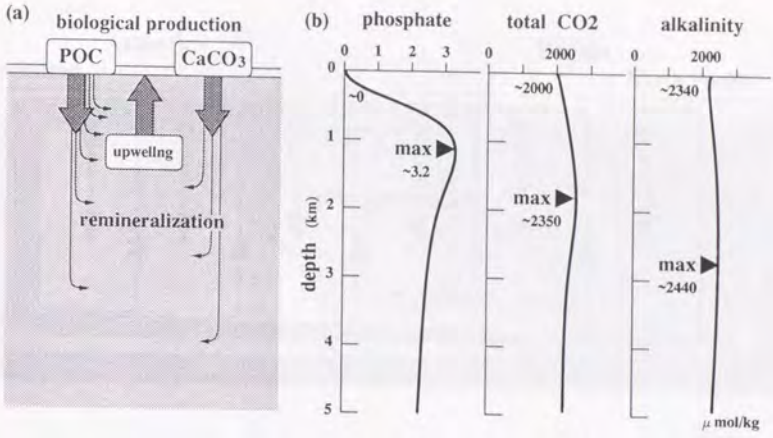

Figure 1-1: The vertical transport and distribution of the chemical tracers: (a) the vertical transport due to biological pump and upwelling and (b) the vertical distribution of phosphate, total CO_2, and alkalinity in the North Pacific.

1.1 Distribution of Chemical Tracers

Distribution of chemical tracers such as phosphate and dissolved oxygen is determined by the biological activity and the ocean circulation. Figure 1-1 illustrates the vertical transport and distribution of the chemical tracers. Part of particulate matter produced by biological activity sinks from the surface to the deep layer. It consists of three components: particulate organic carbon (POC) as soft tissue of organisms, calcium carbonate (mainly as calcite), and silica (opal) as hard parts of organisms. In the deep water, POC, calcite, and opal are remineralized, and the concentration of nutrients, total CO_2, and alkalinity increases. These transport due to sinking particulate matter is generally called the biological pump. The nutrients in the deep water being transported by the upwelling and vertical diffusion return to the surface layer and are consumed by the biological activity. The balance of the transports determines the vertical distribution of the chemical tracers. Almost all of POC is remineralized in the layer shallower than the depth of 1km, and maximum of the phosphate concentration is located at about 1km. On the other hand, almost all of calcite is remineralized on the sea floor, and maximum of the alkalinity concentration is located at about 2~3km, which is deeper than that of phosphate. Total CO_2 concentration increases due to the remineralization of both POC and calcite, and maximum concentration of the total CO_2 is located at the depth between the

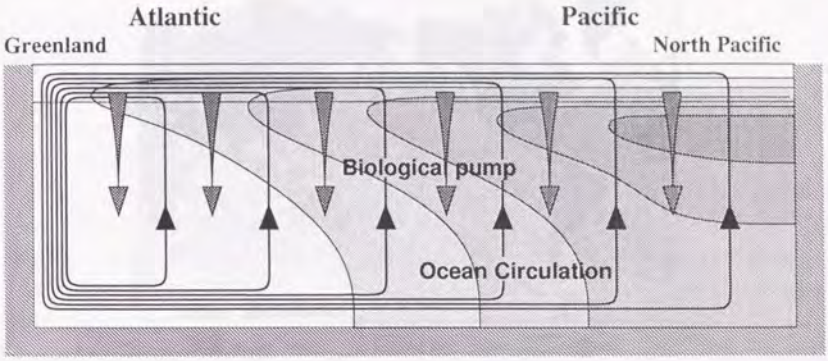

Figure 1-2: The nutrient distribution in the section from the North Atlantic to the North Pacific. This is determined by the ocean circulation and biological pump. Darker shaded area shows the higher concentration of nutrient.

phosphate maximum and the alkalinity maximum. Since dissolved oxygen is consumed when POC is remineralized, the depth of the dissolved oxygen minimum is almost same depth as the phosphate maximum.

In the present ocean, the deep water flows from the North Atlantic to the Pacific and the Indian, while upwelling to the surface layer. This flow pattern is illustrated in Figure 1-2. Vertical nutrient transports due to biological pump and advection/diffusion are dominant in the intermediate layer (about depths of 400m~1km). Horizontal nutrient transport due to advection/diffusion below that layer is also important. The deep water in which POC and calcite are remineralized partly upwells and partly flows toward the North Pacific. That is, the concentration of chemical tracers in the deep water slowly increases due to remineralization of POC and calcite during the pathway to the North Pacific. This is called "conveyor belt", as the deep water carries the precipitated matter from the North Atlantic to the North Pacific [Broecker and Peng, 1982]. This mechanism determines the horizontal distribution of chemical tracers in the deep layer: the concentration in the North Pacific is larger than that in the North Atlantic. Since calcite is remineralized in the layer deeper than POC is, the ratio of horizontal contrast against vertical contrast of alkalinity is larger than that of phosphate.

Marine sediments on the sea floor consists of three major components: calcite and opal as hard parts of organisms, and detritus transported from the continents. Figure 1-3 shows the horizontal distribution of dominant components in the present sediments. The degree of

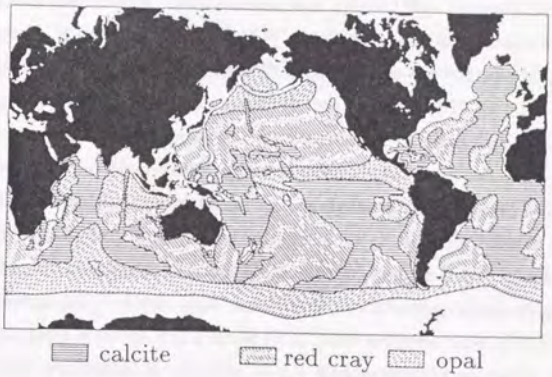

Figure 1-3: The horizontal distribution of dominant components in the present sediments.

saturation for calcite is mainly determined by the pressure dependence of solubility: the depth increases with a decrease in the degree of saturation for calcite. The lysocline is defined as the depth of the saturation horizon for calcite. The calcite is remineralized below the lysocline. The calcite rich sediment is found on shallow sea floor like the mid-ocean ridge. The depth of lysocline decreases from >5km in the North Atlantic to <1km in the North Pacific [Broecker and Takahashi, 1978]. This is because the total CO_2 in the deep water increases owing to an effective remineralization of POC with the flow from the North Atlantic to the North Pacific, and hence the chemical equilibrium, $CO_2 + CO_3^{2-} + H_2O \rightleftharpoons 2\ HCO_3^-$, shifts in the direction of decrease in carbonate ion in this region.

The ocean is everywhere undersaturated for opal. The opal rich sediment is found in the area where the accumulation rate is much higher, like the equatorial Pacific, northern North Pacific, and Southern Ocean. In the deep Atlantic, since silicate poor deep water is transported by upwelling to the surface layer, the opal production due to biological activity and the content of opal in the sediment are lower than in the Pacific and Southern Ocean.

As discussed above, the horizontal distribution of sedimental component is also determined by the biological activity and the ocean circulation.

Carbon in the sea water is roughly categorized into the following three components: dissolved inorganic carbon (DIC), particulate organic carbon (POC), and dissolved organic carbon (DOC). DIC is the largest stock size among the three components, whose concentration is from about 2000μmol/kg in the surface water to about 2400μmol/kg in the deep North Pacific. POC

is the smallest stock size, whose concentration is $< 10\mu$mol/kg. Biomass, such as phytoplankton and zooplankton, is included in POC. POC consists of two components in term of the effect of gravitation, settling POC and suspended POC. Although the concentration of settling POC is $< 0.1\mu$mol/kg, the vertical carbon transport due to settling POC from the surface water to the deep water is much more important for keeping the vertical distribution of DIC, where transport is called the biological pump, as mentioned above.

DOC is strictly defined as one phase of thermodynamics. However, DOC is traditionally defined as the organic carbon that passes through a GF/F filter [Kirchman *et al.*, 1993]. This definition includes several classes of particulate carbon, such as inert colloids and bacteria, all of which pass through GF/F filter. DOC consists of the following three components in term of the utility for biological activity: (1) a labile DOC with turnover time of days or less, (2) semi-refractory DOC (or also called semi-labile DOC) with seasonal time scale, and (3) refractory DOC with extremely long turnover time (centuries or greater) [Kirchman *et al.*, 1993].

1.2 Needs of Study Using Biogeochemical General Circulation Model

A biogeochemical general circulation model (B-GCM) is an ocean general circulation model which is extended to include simple biogeochemical processes. B-GCM can deal not only with current field, temperature, and salinity, but also with various biogeochemical tracers such as nutrients and dissolved oxygen. We can "directly" compare results of simulation by B-GCM with the distribution of the tracers measured a lot by oceanographic expeditions for a long time, and can obtain much more information about the ocean circulation from the study using B-GCM. Since B-GCM can deal with the physical and biogeochemical processes together, we can clarify the role of these processes in determining the distribution of nutrients.

We can also study the carbon cycle by using B-GCM. Since the atmospheric CO_2 level is mainly determined by the partial pressure of CO_2 at the sea surface, the atmospheric CO_2 level can be calculated in a situation different from the present ocean circulation. B-GCM can be a powerful tool for studying variation of the atmospheric CO_2 level in the glacial-interglacial cycle and absorption of anthropogenic CO_2 in the ocean, and can reproduce the environment of sedimentation on the sea floor. B-GCM can also be a powerful tool for the study of paleocean and paleoclimate. The ocean circulation in the paleocean is not directly obtained from the geological data, such as $\delta^{13}C$ obtained from the sediment core, which are limited to the spatial and temporal resolution. The world ocean circulation and global distribution of biological production can be reconstructed from the geological data by using B-GCM. B-GCM is useful to interpret the organic-rich sediments like the anoxic events, as dissolved oxygen can be treated

in B-GCM.

1.3 Previous Studies Using Biogeochemical General Circulation Model

A pioneering study on the ocean carbon cycle using B-GCM was made by Bacastow and Maier-Reimer [1990]. They demonstrated that the distributions of oceanic tracers can roughly be reproduced in their model. The remineralization of POC in their model occurs in the layer much deeper than the depth observed by sediment traps. The minimum concentration of oxygen in their model is not in the northern North Pacific but in the equatorial Pacific, whose value is much lower than observation and whose depth is too deep.

Bacastow and Maier-Reimer [1991] took into account dissolved organic carbon (DOC) in their model, and compared the distribution of phosphate and dissolved oxygen in the model with DOC to that in the model without DOC. They concluded that the model with DOC yields better reproduction of the observed phosphate and dissolved oxygen distributions than that without DOC. Najjar *et al.*[1992] treated only the phosphate cycle in their model. They also concluded that the observed distribution of phosphate is well reproduced only when DOC is included in their model. Although the vertical phosphate distribution in their model with DOC is well compared with the observation, the depth of the thermocline is much deeper than the observed. On the other hand, the vertical phosphate distribution without DOC is similar to that of temperature. These results are considered to be strongly affected by the vertical diffusion. The DOC concentration in Bacastow and Maier-Reimer [1991] and Najjar *et al.*[1992] corresponds to the extraordinarily higher DOC concentration reported by Sugimura and Suzuki [1988] which was withdrawn by Suzuki [1993]. Therefore, DOC concentrations estimated in their models seem to be unrealistically higher than the recent observations [Tanoue, 1992; 1993, Martin and Fitzwater, 1992]. Decay time of their DOC, whose global production rate is about 10GtC/yr, is longer than 50 years, too long to explain the observed seasonal variation of DOC [Carlson *et al.*, 1994].

Najjar *et al.*[1992] pointed out that the concentration of phosphate in a water under high-productivity areas should be higher and the high productivity is maintained by upwelling of this phosphate-rich water. They called this positive feedback mechanism "nutrient trapping".

Recently, Maier-Reimer [1993] improved their model without DOC included. The calculated distributions of tracers have better resemblance with the observation of GEOSECS, although the minimum concentration of oxygen is still not in the northern North Pacific but in the equatorial Pacific. However, the concentration of particulate organic phosphate (POP) at the depth

of 800m in the equatorial Pacific is about 1.5 μmol/l in his model, which is same order as dissolved phosphate and is unrealistically higher than the observed (estimate of the concentration of suspended POP is about $5 \times 10^{-4}\mu$mol/l, which is obtained from the concentration of POC [Druffel *et al.*, 1992])

1.4 Objective and Content of This Thesis

The reason the distribution of chemical tracers is different between the results of the previous models and the observation needs to be clarified. In this thesis, we will discuss the dependency of these distributions on the parameters for biogeochemical processes. DOC treated in the previous studies is not based on the recent observation, and also refractory DOC is not included in the previous studies. New modeling of DOC based on the recent observation is required in order to understand the behavior of DOC. We will develop a B-GCM by taking into account the two components of DOC, semi-refractory DOC and the refractory DOC.

This thesis is organized as follows. In chapter 2, we will develop a B-GCM and clarify the role of the vertical distribution of POC flux in determining the distribution of chemical tracers. The case-studies changing the rain ratio, a ratio of production rate of calcite against that of POC, and the vertical profile of POC flux are made, and the role of these parameters in carbon cycle is discussed. In chapter 3, we will include processes of production and consumption of DOC in B-GCM, whose component is a semi-refractory DOC (S-DOC) and a refractory DOC (R-DOC). The case-studies changing the production rate and the decay time of S-DOC are made, and the role of S-DOC in carbon cycle is discussed. The behavior of R-DOC in carbon cycle is discussed from the distribution of DOC concentration and its Δ^{14}C value in the deep water. In chapter 4, we will give conclusions of this thesis.

This thesis contains three appendices. In appendix A, the chemical reactions in our model are described. In appendix B, five cases changing the vertical diffusion coefficient are run to obtain the optimal value with which the observed distribution of Δ^{14}C is best reproduced. This value is adopted for the studies in chapters 2 and 3. In appendix C, phosphate fluxes between the boxes along the Broecker's conveyor belt in the control case of chapter 2 is calculated. And the cycles of phosphate and the nutrient trapping on the ocean scale are discussed.

References

Bacastow, R., and E. Maier-Reimer (1990): Ocean-circulation model of the carbon cycle., *Clim. Dynamics*, 4, 95-125.

Bacastow, R., and E. Maier-Reimer (1991): Dissolved organic carbon in modeling oceanic new production., *Global Biogeochem. Cycles*, 5, 71-85.

Broecker, W.S., and P.-H. Peng (1982): *Tracers in the Sea.*, Lamont-Doherty Geological Observatory, Palisades, New York.

Broecker, W.S., and T. Takahashi (1978): The relationship between lysocline depth and *in situ* carbonate ion concentration., *Deep Sea Res.*, 25, 65-95.

Carlson, C.A., H.W. Ducklow, and A.F. Michaels (1994): Annual flux of dissolved organic carbon from the euphotic zone in the northwestern Sargasso Sea., *Nature*, 371, 405-408.

Druffel, E.R.M., P.M. Williams, J.E. Bauer, and J.R. Ertel (1992): Cycling of dissolved and particulate organic matter in the open ocean., *J. Geophys. Res.*, 97, 15639-15659.

Kirchman, D.L., C. Lancelot, M. Fasham, L. Legendre, G.Radach, and M. Scott(1993): Dissoled organic matter in biogeochemical models of the ocean., In *Towards a Model of Ocean Biogeochcemical Processes*, NATO ASI Series Vol. I 10, Edited by G.T. Ecans and M.J.R. Facham, pp.209-225., Springer, Berlin.

Maier-Reimer, E. (1993): Geochemical cycles in an ocean general circulation model. preindustrial tracer distributions., *Global Biogeochem. Cycles*, 7, 645-677.

Najjar, R.G., J.L. Sarmiento, and J.R. Toggweiler (1992): Downward transport and fate of organic matter in the ocean: Simulations with a general circulation model., *Global Biogeochem. Cycles*, 6, 45-76.

Sugimura, Y., and Y. Suzuki (1988): A high-temperature catallytic oxidation methods for determination of nonvolatile dissolved organic carbon in seawater by direct injection of a liquid sample., *Mar. Chem.*, 24, 105-131.

Suzuki, Y. (1993): On the measurement of DOC and DON in seeawater., *Mar. Chem.*, 41, 287-288.

Tanoue, E. (1992): Vertical distribution of dissolved organic carbon in the North Pacific as determined by the high-temperature catalytic oxidation method., *Earth Planet. Sci. Lett.*, 111, 201-216.

Tanoue, E. (1993): Distributional characteristics of DOC in the central equatorial Pacific., *J. Oceanog.*, 49, 625-636.

Chapter 2

Role of Vertical Flux of Particulate Organic Carbon in Oceanic Carbon Cycle: Studies Using Ocean Biogeochemical General Circulation Model

Abstract

Distributions of chemical tracers in the world ocean are well reproduced in an ocean general circulation model which includes biogeochemical processes (biogeochemical general circulation model, B-GCM). Both export production and vertically averaged remineralization depth are the factors most sensitive to controlling contrasts of tracer concentrations between the surface and the deep water. Case-studies changing vertical profile of particulate organic carbon (POC) flux show that the phosphate distribution can be reproduced only when the vertical profile of POC flux observed by sediment traps is adopted. The rain ratio, a ratio of production rate of calcite against that of POC, should be smaller than that widely used when the remineralization depth is taken into account, because such a depth of POC is absolutely different from that of calcite. The rain ratio is found to be 0.06~0.08. The export production consistent with the observed distribution of phosphate is estimated to be about 10 GtC/yr.

2.1 Introduction

Oceanic carbon cycle has an important role in controlling the concentration of atmospheric CO_2. It has been widely studied by using various models such as simple box models and three dimensional general circulation models.

A pioneering study on the ocean carbon cycle with an ocean general circulation model which is extended to include biogeochemical processes was made by Bacastow and Maier-Reimer [1990]. They showed that the distributions of oceanic tracers, such as phosphate, dissolved oxygen, alkalinity, total CO_2, and $\delta^{13}C$ can be roughly reproduced in their model, although there were some features which are badly compared with the observation (for example, the depth of phosphate maximum was too deep). Recently, Maier-Reimer [1993] improved their model, and the calculated distributions of tracers have better resemblance with the observation of GEOSECS. Najjar *et al.*[1992] studied phosphate cycling by using their general ocean circulation model, and pointed out that the concentration of phosphate in a water under high-productivity areas should be higher and the high productivity is maintained by upwelling of this phosphate-rich water. They called this positive feedback mechanism "nutrient trapping". However, since the thermocline depth is unrealistically deep in their model, the depth of phosphate maximum is also unrealistically deeper than the observed.

The results of simulation with general circulation models are directly compared with observation. In particular, GCM which is extended to include effects of biogeochemical processes (B-GCM) can deal not only with current field, temperature, and salinity, but also with many biogeochemical tracers such as phosphate and dissolved oxygen. We can obtain much more information about the ocean circulation from the study using B-GCM, as these tracers have been measured a lot by oceanographic expeditions for a long time. Furthermore, the model including isotopes like $\delta^{13}C$ is a useful tool to study not only the present ocean but also the paleo-ocean [Heinze *et al.*, 1991]. It is, however, noted that there are several disadvantages in the study with GCM: for example, a requirement of computer resources and difficulty in interpreting the numerical results compared to the study with simple models.

The partial pressure of carbon dioxide is determined by alkalinity, total CO_2, salinity, and temperature. As shown in Figure 2-1, when we take the global average values of alkalinity and total CO_2, the partial pressure of CO_2 is about 600μatm under the condition of chemical equilibrium at $T = 13°C$ and $S = 35$psu (the global sea surface average). However, alkalinity and total CO_2 in the surface water are generally smaller than the world ocean averages. This is due to biological activities and the ocean circulation. Since the atmosphere is in a dissolution equilibrium with the surface water, the concentration of atmospheric CO_2 is about 300μatm as

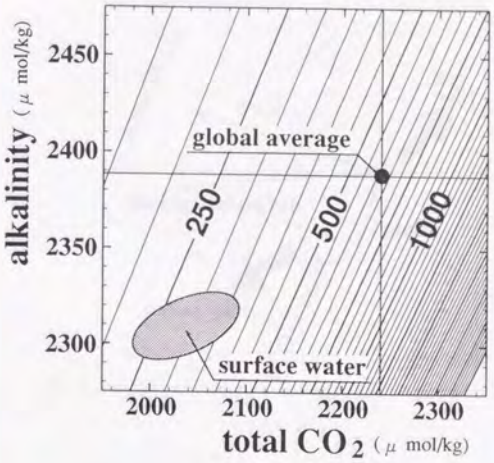

Figure 2-1: Schematic distribution of water mass. Potential pCO_2 (μatm) is a function of total CO_2 (μmol/kg) and alkalinity (μeq/kg) for temperature of 13°C and salinity of 35psu.

it is seen today.

Biological activity also affects distributions of total CO_2 and alkalinity (Figure 2-2). Carbon in the form of particulate organic carbon (POC) as soft tissue of organisms is produced by biological activity in the surface water. As POC sinks from the surface to the deep layer, the concentration of total CO_2 in the surface water decreases and alkalinity slightly increases (the latter is due to consumption of NO_3^-). As a result, the partial pressure of atmospheric CO_2 decreases. Similarly, carbon in the form of calcium carbonate (mainly as calcite) as hard parts of organisms is also produced by biological activity in the surface water. Calcite sinks from the surface to the deep layer, and concentration of total CO_2 and alkalinity in the surface water decreases. As a result, the partial pressure of CO_2 increases. On the other hand, since POC and calcite are remineralized while they are sinking, both total CO_2 and alkalinity in the deep water are generally higher than those in the surface water. Ocean circulation brings up the deep water rich in total CO_2, alkalinity, and also nutrients, which are necessary to biological activity, to the surface layer by upwelling. In this way, the atmospheric CO_2 level and the distributions of total CO_2 and alkalinity in the ocean are determined by the balance between the biological activity and the ocean circulation.

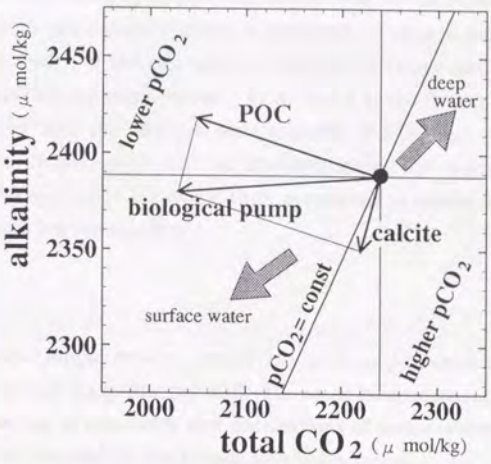

Figure 2-2: Schematic explanation of biological pump. Both total CO_2 and alkalinity in the surface water shift in the direction indicated by arrow of POC (pCO_2 decrease) with production of POC, and in the direction indicated by arrow of calcite (pCO_2 increase) with production of calcite. Combination of the two effects leads to that both total CO_2 and alkalinity in the surface water shift in the direction indicated by the arrow of biological pump, while both total CO_2 and alkalinity in the deep water increase.

As described above, the production and remineralization of POC and calcite affect the carbon cycle in a different way. The ratio of production rate of calcite to that of POC is really important, and it is generally called "rain ratio". When the rain ratio is large, the partial pressure of CO_2 would be high. When it is small, the partial pressure of CO_2 would be low. The rain ratio is estimated to be 0.25 by the two-box model [e.g., Broecker and Peng,1982], and this value has been widely used. However, recent observations provide an estimate of the rain ratio to be much smaller value of 0.11 ± 0.03 [Takahashi *et al.*, 1990]. We will show that the value of the rain ratio should be $0.06 \sim 0.08$.

The role of dissolved organic carbon (DOC) in the oceanic carbon cycle is still controversial. We will not treat DOC in this study. As shown in chapter 3, the effect of DOC on the carbon cycle is limited to the surface layer, roughly above the depth of 400m, and its effect on the distribution of the chemical tracers in the deeper layer below 400m is much weaker than the effect of POC.

In the next section, the model developed in this study will be described. In section 2.3, the vertical transport due to the biological pump is discussed by using a simple model. We will show that the smaller value of the rain ratio is obtained by taking into account the depths at which POC and calcite are remineralized. In section 2.4, the distributions of tracers are obtained for the model with the observed vertical profile of POC flux, and the appropriate rain ratio is presented. In section 2.5, the case-studies changing the rain ratio and the vertical profile of POC flux are made, and the role of these parameters in carbon cycle is discussed. In the final section, results are summarized.

2.2 Model

We develop an ocean biogeochemical general circulation model, which is basically similar to the model of Bacastow and Maier-Reimer[1990]. The ocean biogeochemical general circulation model actually makes use of flow fields and distributions of temperature and salinity of the world ocean, which are obtained by the general circulation model.

2.2.1 General Circulation Model

To obtain the circulation in the world ocean, we use CCSR ocean general circulation model. CCSR model is almost the same as GFDL model [Bryan,1969] for the finite difference scheme except that the weighted upcurrent scheme is adopted for the advection terms of temperature and salinity [Suginohara *et al.*,1991]. The horizontal resolution is four degrees. There are 17 levels in the vertical, whose grid size increases with depth, from 50m for the surface layer to 500m for the deep layers. We adopt the realistic ocean bathymetry, but the Arctic Sea and the Mediterranean Sea are not included (Figure 2-3).

The model is driven by the wind stress and buoyancy forcing at the sea surface. The wind stress used in our model is taken from the annual mean data set of Hellerman and Rosenstein[1983]. As for the buoyancy forcing, temperature and salinity at the sea surface level are restored to the reference values taken from annually averaged data sets of Levitus[1982]. However, since the North Atlantic Deep Water (NADW) becomes weak under the annual mean condition of sea surface temperature, we take a reference temperature which is 4K cooler than the annual mean condition at 60°N (this corresponds to the mid-winter condition) and decreases linearly from 50°N to 60°N. As a result, we obtained the transport of NADW comparable with the observation (see Section 2.4).

Initial conditions are no motion and horizontally uniform distribution of temperature and salinity. After carrying out the time integration for 10,000 years, we obtain flow fields and

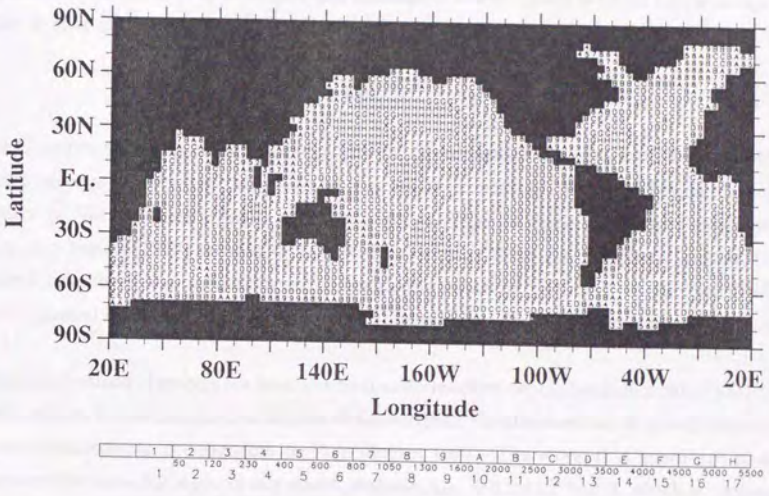

Figure 2-3: Bathymetry.

distributions of temperature and salinity which can be regarded as a steady state.

2.2.2 Biogeochemical General Circulation Model

Prognostic Variables and Mass Conservation

Prognostic variables in our B-GCM are concentrations of atmospheric CO_2, oceanic total CO_2, alkalinity, phosphate, and dissolved oxygen. Concentrations of these tracers are calculated as the forms normalized by salinity of 35psu, as the effects of water evaporation and precipitation are ignored in this model. The fact that the mixing process of CO_2 in the atmosphere is much faster than that in the ocean allows the atmosphere to be treated as one box.

^{13}C is treated as an individual tracer, and hence $^{13}CO_2$ in the atmosphere and total $^{13}CO_2$ in the ocean are also prognostic variables. Although ^{14}C is not dealt with as an individual tracer, we consider it in the form of $\Delta^{14}C$ according to the method of Toggweiler *et al.*[1989].

Sedimentation processes and river input due to the continental weathering are not included in our model. Therefore, the total amounts of ^{12}C and ^{13}C are conserved in the atmosphere-ocean system. Similarly, the total amounts of phosphate and alkalinity are conserved in the ocean.

Physical Process

Dynamic processes such as advection and diffusion of tracers in our B-GCM follow an equation similar to that used in the circulation model:

$$\frac{\partial C}{\partial t} + \boldsymbol{u} \cdot \nabla C = A_{HH} \nabla_H^2 C + A_{HV} \frac{\partial^2 C}{\partial z^2} + S_C, \qquad (2-1)$$

where C represents a concentration of each tracer, S_C represents a source term due to biological process, and $\boldsymbol{u}$ is current velocity. A_{HH} and A_{HV} are horizontal and vertical diffusion coefficients, respectively. We assume the same values for A_{HH} and A_{HV} as those in the circulation model.

Kuo and Veronis[1973] estimated $A_{HH} = 6 \times 10^2 \mathrm{m}^2/\mathrm{s}$ from the horizontal distribution of dissolved oxygen in the abyssal layer, although the value on the order of $10^3 \sim 10^4 \mathrm{m}^2/\mathrm{s}$ is usually adopted in the GCM to avoid numerical instability. We take $A_{HH} = 8 \times 10^2 \mathrm{m}^2/\mathrm{s}$ in our model.

The distributions of tracers are sensitive to the thermocline depth, because most of particulate organic carbon is remineralized at depths shallower than the thermocline. It is well known that the thermocline depth is dependent on A_{HV} [Bryan, 1987]. Therefore, it is important to adopt an appropriate value for A_{HV}. In our model, we take $A_{HV} = 0.2 \times 10^{-4} \mathrm{m}^2/\mathrm{s}$, which is comparable with observation [e.g., Ledwell *et al.*, 1993].

Chemical Process and Gas Exchange

The chemical and biological processes considered in our model are illustrated in Figure 2-4. The surface partial pressure of carbon dioxide pCO_2 is derived from alkalinity, total CO_2, temperature, and salinity under the condition of chemical equilibrium. Alkalinity is determined in the carbon-borate-water system, where the total amount of borate is given as a linear function of salinity. The apparent dissociation constants for carbon, borate, and water are taken from Dickson and Millero[1987], Johansson and Wedborg [1982], and Dickson and Riley [1979]. The solubility of carbon dioxide is taken from Weiss [1974]. Gas exchange of CO_2 through the sea surface is assumed to be proportional to the difference of pCO_2 between the atmosphere and the surface ocean. The gas exchange coefficient is assumed to be globally uniform at $K = 0.06$ mol/(m^2 yr μatm) [Maier-Reimer, 1993].

It is known that the partial pressure of carbon dioxide in the atmosphere is not locally in equilibrium with that in the ocean. Therefore, we consider not an equilibrium fractionation factor but one-way fractionation factors for carbon exchange from the ocean to the atmosphere and from the atmosphere to the ocean as functions of temperature and concentrations of carbon dioxide, bicarbonate ion, and carbonate ion. The details of treatments of fractionation process of carbon isotope through the gas exchange are described in Appendix.

The concentration of dissolved oxygen in the surface water is restored to be 3% super satu-

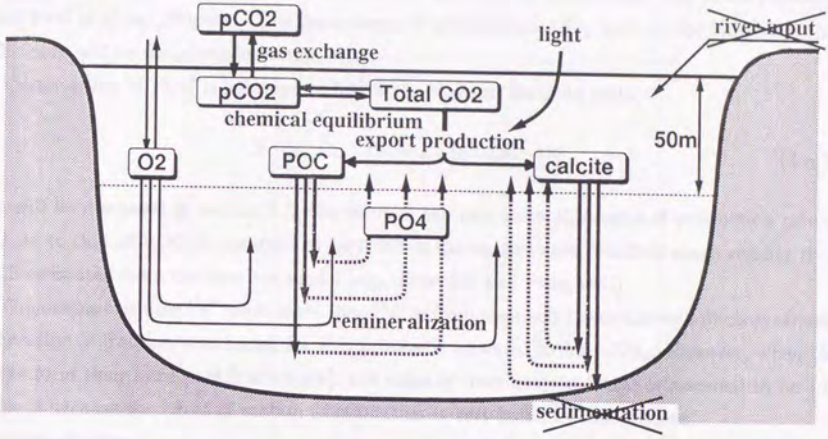

Figure 2-4: Chemical and biological processes considered in the Biogeochemical-GCM. Processes of sedimentation and river input are not included.

ration in a restoring time of 17 days [Broecker & Peng, 1982]. The value of saturation is taken from Weiss[1970].

Export Production

Photosynthesis and hence biological production take place only in the surface layer of the ocean. Export production EP is assumed to be a function of phosphate concentration $[PO_4]$ and light factor L_f as follows:

$$EP = r D_e L_f \, [PO_4] \frac{[PO_4]}{h + [PO_4]} \qquad (2-2)$$

where h is a half-saturation constant, D_e is a depth of the surface layer, and r is a proportional factor(we call this "bio-production efficiency"). The light factor L_f is proportional to an annually averaged solar radiation, which is a simple function of latitude and is normalized to be $0 \leq L_f \leq 1$. The dependency of phosphate concentration on EP is assumed to follow Michaelis-Menten kinetics [Maier-Reimer, 1993]. Since phosphate concentration in the surface water is usually much larger than half-saturation constant of 0.02μmol/L [Maier-Reimer, 1993], we approximate EP to be a linear function of $L_f[PO_4]$. As Maier-Reimer [1993] mentioned, the distributions of chemical tracers depend strongly on the bio-production efficiency. In this

study, we use $r = 1.0\ \mathrm{yr}^{-1}$, which is obtained by adjusting the atmospheric CO_2 to the preindustrial level of about 280μatm. The dependency of atmospheric CO_2 level on the bio-production efficiency will be described in section 2.5.

Composition of POC is assumed to follow the classical Redfield ratio,

$$\mathrm{P} : \mathrm{N} : \mathrm{C} : -\mathrm{O}_2 = 1 : 16 : 106 : 138. \qquad (2-3)$$

As will be discussed in section 2.3, the value of the rain ratio R, a ratio of production rate of calcite to that of POC, is assumed to be 0.045 in the control case, which is much smaller than 0.25 estimated from the two-box model [e.g., Broecker and Peng,1982].

Organisms consume ^{12}C much more than ^{13}C to form their soft tissue through photosynthesis. The value of fractionation factor for this process is assumed to be $-22‰$. However, when the biota form their hard part (carbonate), the value of fractionation factor is assumed to be 1.0. This is because the effect of carbon fractionation is very small in this process.

Remineralization

POC is assumed to be remineralized instantaneously below the euphotic zone. Horizontal advection of POC will be negligible, as settling speed of POC is about 100m/day [Suess *et al.*, 1980], which is much faster than the horizontal advection.

The vertical profiles of vertical fluxes of POC and calcite assumed in our model are shown in Figure 2-5. In each case, the vertical profile of POC flux is represented in the form of $(z/100\mathrm{m})^a$. Case studies are performed for the three profiles : $a = -0.988$ (control case), $a = -2.0$ (shallow profile case), and $a = -0.4$ (deep profile case). The profile used in the control case is taken from vertical flux of particulate organic nitrate obtained from the sediment traps [Martin *et al.*, 1987]. This profile is also similar to the profile of POC flux observed by Suess *et al.*[1980]. The expression of vertical profile as $(z/100\mathrm{m})^a$ was originally proposed by Martin *et al.*[1987] who determined it from sediment trap data at depths shallower than 2000m. But this gives an unrealistically uniform distribution below the depth of 2000m. Since sedimentation process is not included in our model, all POC reached the bottom should be remineralized. Therefore, we modify the original form for the vertical profile of POC as $(z/100\mathrm{m})^a f$, where f is one above the depth of 1500m, and decreases linearly from one at 1500m to zero at 5500m. However, as will be discussed in section 2.5, f does not significantly affect the characteristic features of the results such as a depth of phosphate maximum.

Dissolution of POC under anoxic condition may be important for the distribution of tracers especially in the eastern equatorial Pacific and the Gulf of Guinea. We consider three treatments for POC dissolution under such a condition. The first treatment is that POC passes trough the

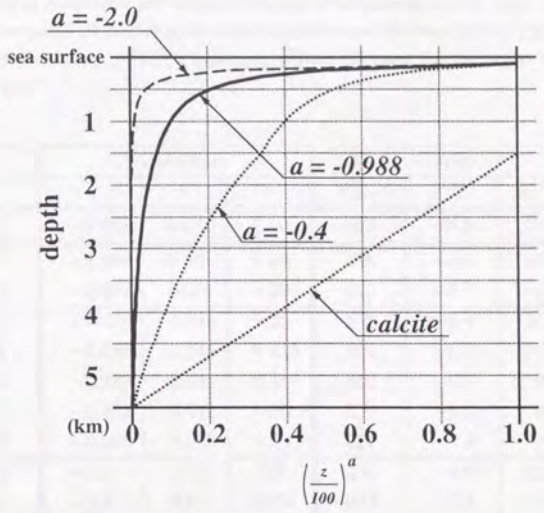

Figure 2-5: Vertical profiles of POC flux and calcite flux used in the Biogeochemical-GCM.

anoxic layer and is remineralized below it. The second is that the POC is always remineralized even in the anoxic or the euoxic layer. In this case, we permit a negative value for dissolved oxygen concentration. The third, as was adopted by Bacastow and Maier-Reimer [1990], is that POC is basically not remineralized in the anoxic layer, although the amount estimated by the second treatment is remineralized as long as the dissolved oxygen is abundant.

These treatments strongly affect the concentrations of tracers in the eastern equatorial Pacific, but do not affect much in other regions in the control profile case. We choose the first treatment as a standard in this study. This issue may be solved partly by taking into account the Fasham-type plankton model [Maier-Reimer, 1993] or studied in chapter 3 in the B-GCM. However, this is for the future study.

Since the sedimentation process is not included in our model, calcite is assumed to dissolve uniformly below the depth of 1500m.

Initial Condition and Time Integration

As an initial condition, the concentration of tracers are assumed to be homogeneous in the whole ocean. The concentration of phosphate is taken to be 2.1 μmol/kg, which corresponds

Table 2-1: Summary of parameters and results of numerical experiments in this study. a is an exponent appeared in the POC flux profile, R the rain ratio, r the bio-production efficiency (yr^{-1}), CO_2 the partial pressure of CO_2 in the atmosphere (μatm), $\delta^{13}C$ ^{13}C in the atmosphere (‰), and EP the export production(GtC/yr). Exp.1 is the control case.

Exp.	parameters			results		
	a	R	r	CO_2	$\delta^{13}C$	EP
1	−0.988	0.045	1.00	283	−6.5	10.3
2	−0.988	0.12	1.00	328	−6.6	10.3
3	−0.988	0.25	1.00	443	−6.7	10.3
4	−0.988	0.045	1.25	271	−6.4	10.5
5	−0.988	0.045	0.825	294	−6.6	10.0
6	−0.988	0.045	0.75	300	−6.7	9.8
7	−0.988	0.045	0.50	326	−6.9	8.6
8	−0.988	0.045	0.25	327	−7.3	6.1
9	−2.0	0.02	1.50	288	−6.6	15.3
10	−2.0	0.02	0.75	334	−7.6	12.8
11	−0.4	0.12	0.375	285	−6.5	4.6
12	no biota			483	−8.0	0

to the average of observed values in the world ocean [Levitus *et al.*, 1993]. Similarly, the alkalinity is taken to be 2374 μeq/kg [Takahashi *et al.*, 1981]. The total CO_2 is assumed to be 2235 μmol/kg which is near at the preindustrial level (we estimate the preindustrial level to be 2239 μmol/kg from the amount of anthropogenic CO_2 release and the present value of 2254 μmol/kg [Takahashi *et al.*, 1981]). The partial pressure of atmospheric CO_2 is assumed to be the preindustrial value of 280 μatm. The amount of ^{13}C is also assumed to be the preindustrial value, which is equivalent to $\delta^{13}C = -6.5$‰ in the atmosphere and $\delta^{13}C = 0.4$‰ in the ocean [Kroopnick, 1985]. Dissolved oxygen is assumed to be 200 μmol/kg.

We performed twelve-case studies. Parameters and results in these cases are listed in Table 1. We obtain the distribution of tracers for each case, after carring out the time integration for the 3000 years, which is considered to be long enough for achieving a steady state.

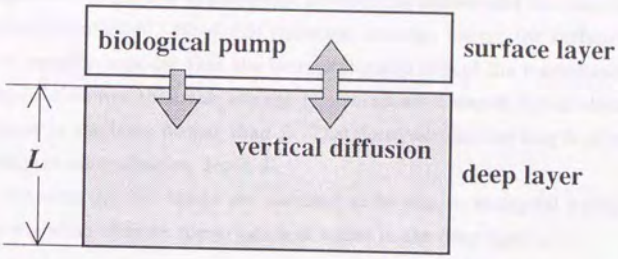

Figure 2-6: Two-box model for understanding the biological pump.

2.3 Biological Pump

Before showing the numerical results, we discuss the vertical transport of biogenic particulates such as POC and carbonates. This is generally called the biological pump.

2.3.1 Strength of Biological Pump

An efficiency of vertical transport due to the biological pump is determined not only by the export production but also by the depth where biogenic particulates are effectively remineralized. In other words, this efficiency depends on the amount of particulate produced by biological activity and also on the effective length of vertical transport.

We define the strength of biological pump I, which is an index for the efficiency of vertical transport, as follows:

$$I = \int_{z_b}^{z_s} z \frac{dF(z)}{dz}\, dz, \qquad (2-4)$$

where z represents depth ($z = z_s$ is the bottom of euphotic layer and $z = z_b$ is the bottom of the ocean), and $F(z)$ is the vertical flux of settling biogenic particulate.

We also define the average remineralization depth L as the strength of biological pump divided by the export production, that is,

$$L \equiv \frac{I}{EP}, \qquad (2-5)$$

where EP is the export production. In the control case ($a = -0.988$), the average remineralization depths of POC and calcite are $L_{\mathrm{POC}} = 540$m and $L_{\mathrm{calcite}} = 3500$m, respectively.

Here we discuss the relation between the strength of biological pump and the difference in

the concentration of tracers such as phosphate between the surface and the deep layer, by using a two-box model (Figure 2-6). We divide the ocean into two boxes: the surface and the deep layers. We can roughly consider that the biological pump affects the concentration of tracers in the deep layer shallower than the average remineralization depth L, but doess not change the concentration in the layer deeper than L. Therefore, we take the length of the deep layer to be the average remineralization depth L.

The fluxes between the two boxes are assumed to be due to biological pump and vertical diffusion. The equation of mass conservation of tracer in the deep layer is

$$L\frac{dC}{dt} = EP - \frac{k\Delta C}{L}, \tag{2-6}$$

where ΔC is the difference of concentrations of tracer between two boxes, and k represents the vertical diffusion coefficient. Then, in a steady state, we obtain the following relation,

$$I = EP \times L = k\Delta C. \tag{2-7}$$

The strength of biological pump is proportional to the difference of concentrations between the surface and the deep layer. This means that the difference in concentration depends not only on the export production but also on the depth where biogenic particulate is remineralized. Although the effects of vertical advection and horizontal diffusion/advection are not considered in the above discussion, this expression will be appropriate for the real ocean, as discussed in section 2.5.

2.3.2 Rain Ratio

The ratio of the difference of total CO_2 concentrations between the surface and the deep layer ($= \Delta[TCO_2]$) to that of alkalinity ($= \Delta[Alk]$) is 3$\sim$4. It is known that this ratio is accounted for by the two-box model with the rain ratio of 0.25 [e.g., Broecker and Peng, 1982]. The differences in both total CO_2 and alkalinity are determined by dissolutions of POC ($= \Delta C_{POC}$) and calcite ($= \Delta C_{calcite}$) in the deep water as follows:

$$\begin{aligned} \Delta[TCO_2] &= \Delta C_{POC} + \Delta C_{calcite} \\ \Delta[Alk] &= -\frac{16}{106}\Delta C_{POC} + 2\Delta C_{calcite}, \end{aligned} \tag{2-8}$$

that is,

$$\frac{\Delta C_{calcite}}{\Delta C_{POC}} = \frac{16/106(\Delta[Alk]/\Delta[TCO_2]) + 1}{2(\Delta[Alk]/\Delta[TCO_2]) - 1} \simeq 0.25. \tag{2-9}$$

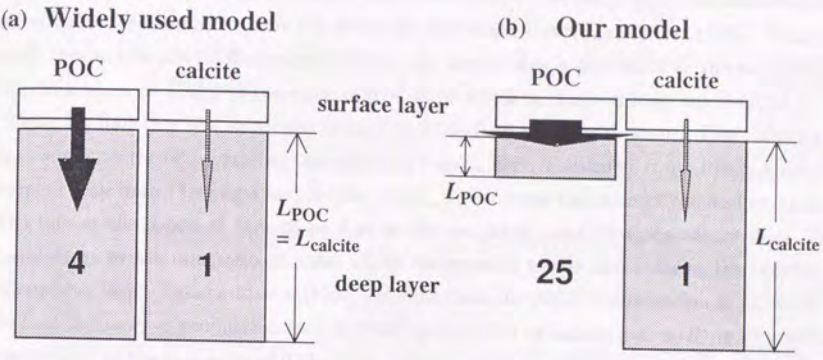

Figure 2-7: The difference between the widely used model and ours.

Figure 2-7 shows the widely used two-box model and ours. In the two-box model proposed in Figure 2-7(a), the average remineralization depth of POC and that of calcite are implicitly assumed to be the same (i.e., $L_{\rm POC} = L_{\rm calcite}$). However, in the real ocean, $L_{\rm POC}$ is much shallower than $L_{\rm calcite}$, and thus we must consider the difference of the average remineralization depths (Figure 2-7b). We therefore modify the rain ratio R as follows:

$$R \equiv \frac{EP_{\rm calcite}}{EP_{\rm POC}} = \frac{I_{\rm calcite}}{I_{\rm POC}} \frac{L_{\rm POC}}{L_{\rm calcite}} = \frac{\Delta C_{\rm calcite}}{\Delta C_{\rm POC}} \frac{L_{\rm POC}}{L_{\rm calcite}} \simeq 0.25 \times \frac{L_{\rm POC}}{L_{\rm calcite}}. \qquad (2-10)$$

Since $L_{\rm POC}$ and $L_{\rm calcite}$ in the control case are estimated to be 540m and 3500m, respectively, the rain ratio is expected to be about 0.04, which is much smaller than the value of 0.25 estimated by the widely used two-box model.

For application of this result to the real ocean, we must note the following two points. First, a two-box model is too simple to be directly applied to the real ocean. In fact, $R = 0.04 \sim 0.06$ is obtained as the most reasonable estimate from our B-GCM, as will be discussed in section 2.5. This value is much more likely than the value estimated from the simple two-box model. Second, the sedimentation and the river input processes are not included in our model. Even when we take into account these processes, the total amount of tracers in the ocean is conserved in a steady state, as the river input rate is balanced with the sedimentation rate. However, since the production rate of calcite is balanced with its remineralization rate (which is included in our model) and its sedimentation rate (which is not included), the production rate of calcite obtained in our model should be underestimated. We must include the contribution of carbonate

sedimentation to the rain ratio in order to apply our model to the real ocean. The sedimentation rate of calcite is estimated to be 0.2 Gt/yr for the world ocean [Sundquist, 1985]. With the export production of 10.3 Gt/yr estimated in our model, this is equivalent to the rain ratio of 0.02. This must be added to the value of 0.04∼0.06 which is obtained from our B-GCM.

Thus, we find that the rain ratio should be 0.06∼0.08 in the real ocean. This estimate is consistent with the observations [Tsunogai and Noriki, 1991; Takahashi *et al.*, 1990]. From the sediment trap data [Tsunogai and Noriki, 1991], we estimate the ratio of calcite flux against POC flux at the depth of 1km to be 0.51 as the weighted mean by using calcite flux. This is equivalent to the rain ratio of 0.056 which corresponds to the rain ratio at the bottom of the euphotic layer. Takahashi *et al.*[1990] reported from the JGOFS observation at 47°N-20°W site that the ratio of production rate of POC against that of calcite (i.e. $1/R$) is 9±2, which is equivalent to the rain ratio of 0.11±0.03. All these observational estimates roughly coincide with our estimate. Therefore, the rain ratio is around 0.06∼0.08, which is obviously much smaller than 0.25 estimated by the widely used two-box model.

Bacastow and Maier-Reimer[1990] used the rain ratio of 0.15. This is probably because their POC flux was assumed to be remineralized at the depths deeper than those estimated from the observed POC flux. In Maier-Reimer [1993], the rain ratio was given as a function of temperature. He reported the global average of the rain ratio to be 0.22, which is close to 0.25. However, this value seems to be obtained by an spatially weighted mean. Since the rain ratio was very small in the high productivity region whereas total fluxes are very large there, the value estimated from the total production rate of POC and that of calcite for the world ocean would be smaller than 0.22.

2.4 Results

In this section, we describe the results of the control case (Exp.1) of our biogeochemical general circulation model.

Physical Fields

Figures 2-8(a) through 2-8(f) shows that meridional mass transport and distributions of temperature and salinity in the Atlantic and the Pacific meridional sections.

Stream function of meridional mass transport in the Atlantic and the Pacific is shown in Figures 2-8(a) and 2-8(b), respectively. In the Atlantic, the maximum transport of NADW is 24Sv ($= 24 \times 10^6 \mathrm{m}^3/\mathrm{s}$), and the outflow from the Atlantic is 17Sv. As was stated in section 2.2, we use the reference sea surface temperature lower than the annual condition for the northern North Atlantic so that the transport of NADW may be comparable with the observation [e.g.,

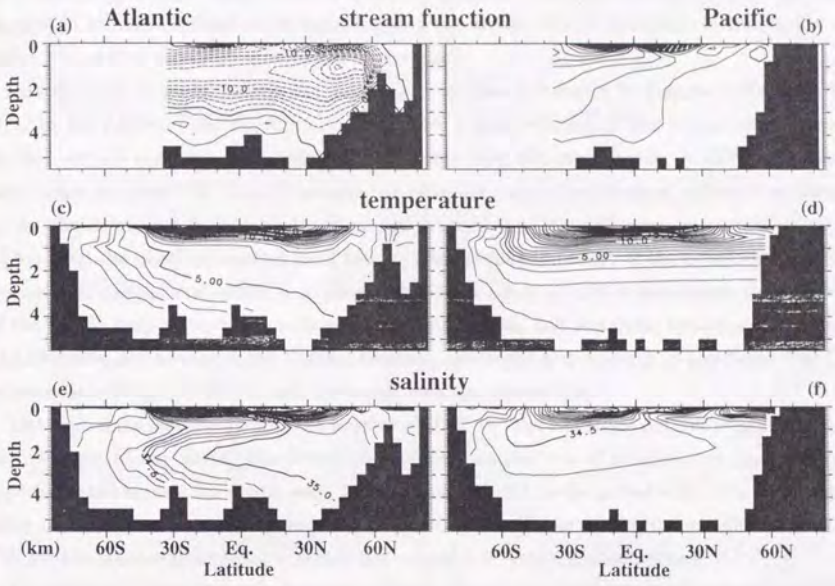

Figure 2-8: Results of the physical fields. Meridional mass transport stream function for (a) the Atlantic and (b) the Pacific. Contour interval is 2Sv (1Sv=$10^6 m^3$/sec). Meridional sections of temperature along (c) the GEOSECS western Atlantic and (d) the GEOSECS western Pacific. Contour interval is 1K. Meridional sections of salinity along (e) the GEOSECS western Atlantic and (f) the GEOSECS western Pacific. Contour interval is 0.1psu.

Rintoul, 1991]. The maximum transport of the Antarctic Bottom Water (AABW) is 4Sv. In the Pacific, the inflow below the depth of 2km is 6Sv. This is considered to be slightly smaller than the real ocean, as the meridional contrast of $\Delta^{14}C$ in the deep water is stronger than the GEOSECS observation, which will be discussed later. The Ekman circulation, a meridional circulation driven by wind stress, is limited to the layer above the depth of 500m.

Distributions of temperature along GEOSECS sections in the western Atlantic and the western Pacific are shown in Figures 2-8(c) and 2-8(d). The isotherm of 10°C lies at about 500m depth in the Atlantic and the Pacific, and the isotherm of 5°C lies at about 1000m in the Pacific. The thermocline depth both in the Atlantic and the Pacific is well reproduced, which is due to the small value for the vertical diffusion coefficient adopted in our model. The temperature

of NADW is about 2K warmer than the observed because the cold overflow water across the straight of Iceland-Scotland is not reproduced in our model. The temperature in the Pacific is about 1°C, which is consistent with the observation.

Distributions of salinity along the GEOSECS sections are shown in Figures 2-8(e) and 2-8(f). In the Atlantic, the salinity minimum water is well reproduced due to the small values for the vertical and horizontal diffusion coefficients. On the other hands, AABW is far less saline than the observed. This is because the reference value of sea surface salinity was taken as the annual mean condition for the Ross and Weddell Seas (the reference sea surface salinity higher than the observed is often used to take into account the effect of the brine rejection by sea-ice formation in mid-winter [e.g., England, 1993]). Since AABW is less saline, the salinity of the Pacific deep water becomes lower than the observed, and Antarctic Intermediate Water (AAIW) does not appear in the Pacific. However, the depth and strength of the North Pacific Intermediate Water(NPIW) is well compared with the observation.

Although some features such as the warmer NADW and the less saline AABW require further improvement of the model, the flow fields and the distributions of temperature and salinity, especially the thermocline depth, seem to be well reproduced on the global scale. The maximum value of meridional heat transport is 1.4 PW ($= 10^{15}$W) for the northern hemisphere and 1.6 PW for the southern hemisphere, which are comparable with the observations.

Figures 2-9(a) through 2-9(l) show the distributions of the various chemical tracers along the GEOSECS sections in the western Atlantic and the western Pacific.

Distribution of $\Delta^{14}C$

The distributions of Δ^{14}C along the GEOSECS sections are shown in Figures 2-9(a) and 2-9(b). Δ^{14}C is a passive tracer and its distribution is determined only by the flow fields and decay time, although the gas exchange between the atmosphere and the ocean has some influence. Therefore, the distribution of Δ^{14}C is useful for understanding the abyssal circulation.

The values of Δ^{14}C of the deep water in the North Atlantic and the North Pacific are $-60‰$ and $-250‰$, respectively, which are well compared with the observation [Stuiver and Ostlund, 1980; Ostlund and Stuiver, 1980]. Since the flow is slightly stronger in the Atlantic, the value of Δ^{14}C in the Southern Ocean becomes younger than the observed.

Distributions of Phosphate and Dissolved Oxygen

Figures 2-9(c) and 2-9(d) show the distributions of phosphate along the GEOSECS. The phosphate maximum is found at about 1200m depth in the Pacific and at about 800m depth in the Atlantic, which is well compared with the observation. In the Atlantic, this maximum seems to spread as a tongue from the Southern Ocean. The maximum value of 3.3 μmol/kg is found in the northern part of the North Pacific. This is comparable with the observed value of

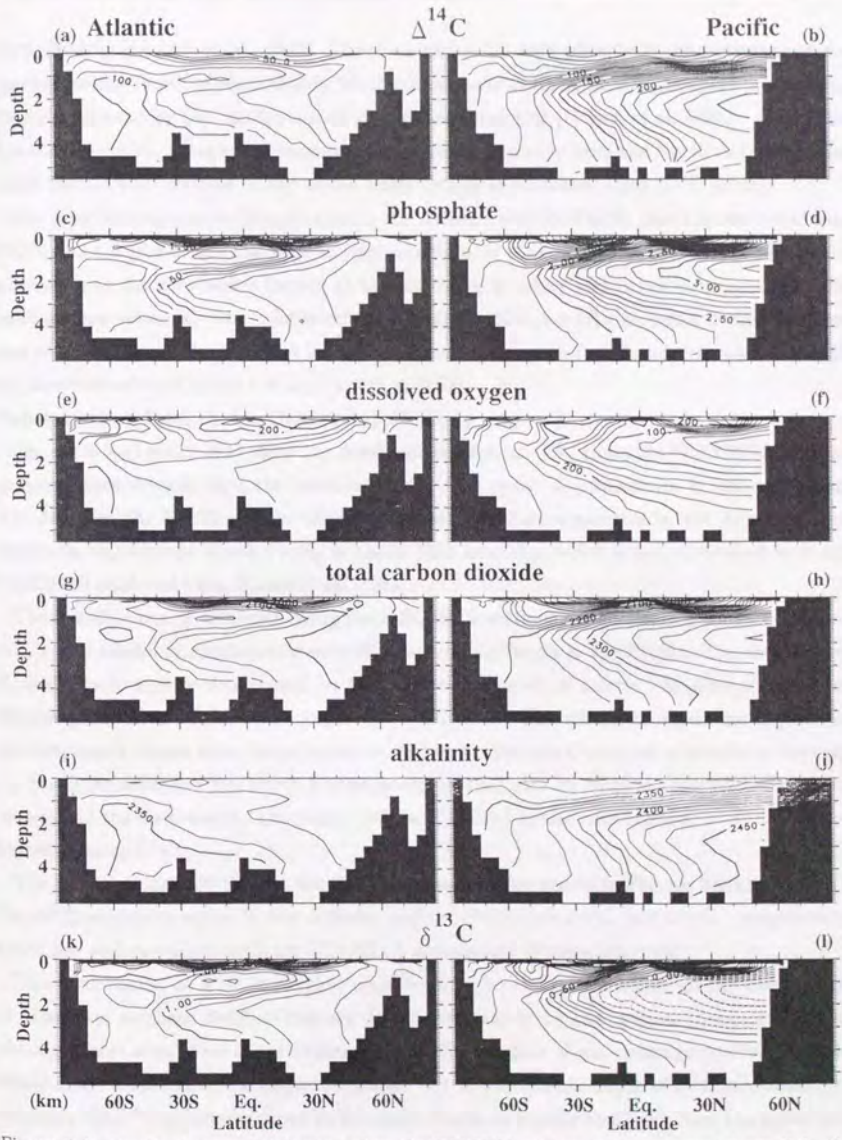

Figure 2-9: Results of tracer distributions along the GEOSECS sections in the western Atlantic (left side) and the western Pacific (right side). Δ^{14}C (a,b; contour intervals = 10‰), phosphate (c,d; contour intervals = 0.1μmol/kg), dissolved oxygen (e,f; contour intervals = 20μmol/kg), total CO_2 (g,h; contour intervals = 20μmol/kg), alkalinity (i,j; contour intervals = 10μeq/kg), δ^{13}C (k,l; contour intervals = 0.1‰).

>3.2 μmol/kg [Levitus *et al.*, 1993]. There are regions of high phosphate concentration above the thermocline depth of about 500m, which corresponds to the area of high export production. This is explained by the mechanism of the nutrient trapping [Najjar *et al.*, 1992]. Below the thermocline depth, phosphate concentration increases gradually from the North Atlantic to the North Pacific with increase in age of the water (which is estimated from $\Delta^{14}C$ value).

The dissolved oxygen minimum exists in the Atlantic and the Pacific (see Figures 2-9(e) and 2-9(f)). The depth of the dissolved oxygen minimum is shallower than that of the phosphate maximum, as the deep water formed at high latitudes is colder and richer in oxygen than the usual surface water is. The minimum value of about 30.0 μmol/kg is found in the northern part of the Northern Pacific. This value corresponds to about 0.7 ml/l and is comparable with the observed value of about 0.6 ml/l [Levitus, 1982].

Distributions of Total Carbon Dioxide and Alkalinity

Figures 2-9(g) and 2-9(h) show the distributions of total CO_2 along the GEOSECS sections in the western Atlantic and the western Pacific. The total CO_2 maximum is found at about 2km depth in the Pacific and in the layer of the phosphate maximum in the Atlantic. The maximum value in the North Pacific is about 2400 μmol/kg, which is well compared with the GEOSECS observed value [Craig *et al.*, 1981].

The distributions of alkalinity along the GEOSECS sections are shown in Figures 2-9(i) and 2-9(j). The alkalinity maximum is seen at about 2~3km depth in the Pacific. The distribution of alkalinity is mainly determined by the vertical transport of calcite. In general, calcite is effectively dissolved in the layer deeper than POC does. The alkalinity maximum appears in the layer much deeper than the phosphate maximum. Horizontal contrast of alkalinity between the North Atlantic and the North Pacific is comparable with its vertical contrast between the surface and the deep water. The reason will be discussed in the next section.

Distribution of $\delta^{13}C$

The distributions of $\delta^{13}C$ along the GEOSECS sections are shown in Figures 2-9(k) and 2-9(l). The $\delta^{13}C$ minimum values in the Atlantic and the Pacific are 0.7‰ and -0.6‰ , respectively, which are well compared with the GEOSECS observation [Kroopnick, 1985].

The distribution of $\delta^{13}C$ is roughly considered to be the mirror image of the distribution of phosphate as these distributions are determined mainly by the vertical transport of POC although there is an effect of gas exchange on $\delta^{13}C$. The effect of gas exchange on $\delta^{13}C$ distribution is much weaker than the biological pump. But this affects the depth of $\delta^{13}C$ minimum. For example, the $\delta^{13}C$ minimum depth in the north Pacific is slightly shallower than the phosphate maximum. The reason is as follows: the fractionation of carbon isotopes through gas exchange is larger for lower temperature, that is, the sea water at low temperature becomes much more

^{13}C-rich than the sea water at high temperature. Since production of deep water occurs at high latitudes, the deep water is richer in ^{13}C than that in the surface water at low and middle latitudes. Therefore, the $\delta^{13}C$ minimum is formed at the depths shallower than the phosphate maximum layer.

The atmospheric $\delta^{13}C$ becomes $-6.50‰$, which is equal to the preindustrial value [Kroopnick, 1985].

Horizontal Distribution of ΔpCO_2

The partial pressure of CO_2 in the atmosphere is 283 μatm, which coincides with the preindustrial value. Figure 2-10 shows the distribution of ΔpCO_2 which represents the difference in partial pressure of CO_2 between the atmosphere and the ocean. Figures 2-10(a) and 2-10(b) are for the observation by Tans *et al.*[1990], and Figure 2-10(c) for our results. Since the simulation is performed under the annual mean condition and that for the preindustrial state, direct comparison of ΔpCO_2 between the model results and the observation may be difficult. Here, we make a rough comparison for the features in ΔpCO_2 distribution. In the equatorial Pacific, pCO_2 in the ocean is >100 μatm higher than that in the atmosphere due to the upwelling of the deep water with high pCO_2. In the subtropical region, the oceanic pCO_2 is lower than the atmospheric pCO_2 by the effect of biological pump. In the northern North Atlantic, pCO_2 of the sea water is much lower than that of the atmosphere, as NADW exports the total CO_2 out of this region in association with the formation of deep water. The high and the low pCO_2 regions appeare to spread, somewhat randomly, over the other area at high latitudes. In the area of high pCO_2, the CO_2-rich water is brought up from the sub-surface layer by convection.

Distribution Potential pCO_2 and Degree of Calcite Saturation

Potential pCO_2 is defined as the CO_2 pressure that would be achieved if the water were brought up isochemically to the surface at the global average surface temperature, T=13°C, and salinity, S=35psu [Broecker and Peng, 1982]. Figure 2-11 shows the distributions of potential pCO_2 along the GEOSECS sections in the western Atlantic and the western Pacific.

As mentioned in section 2.1, the potential pCO_2 for the world ocean at the averaged alkalinity and total CO_2 is about 600μatm. In fact, although the value of potential pCO_2 in the deep Atlantic is lower than 600μatm(Figure 2-11(a)), that in the deep Pacific except the Southern Ocean is higher than 600μatm (Figure 2-11(b)). In particular, the potential pCO_2 at the depth of 1km in the North Pacific is estimated to be about twice the value of the world ocean average owing to an effective dissolution of POC into this water mass. As a result, the distribution of potential pCO_2 is similar to that of phosphate. Below the depth of 2km, the potential pCO_2 decreases because of dissolution of calcite.

Figure 2-12 shows the degree of saturation with respect to calcite estimated from *in situ*

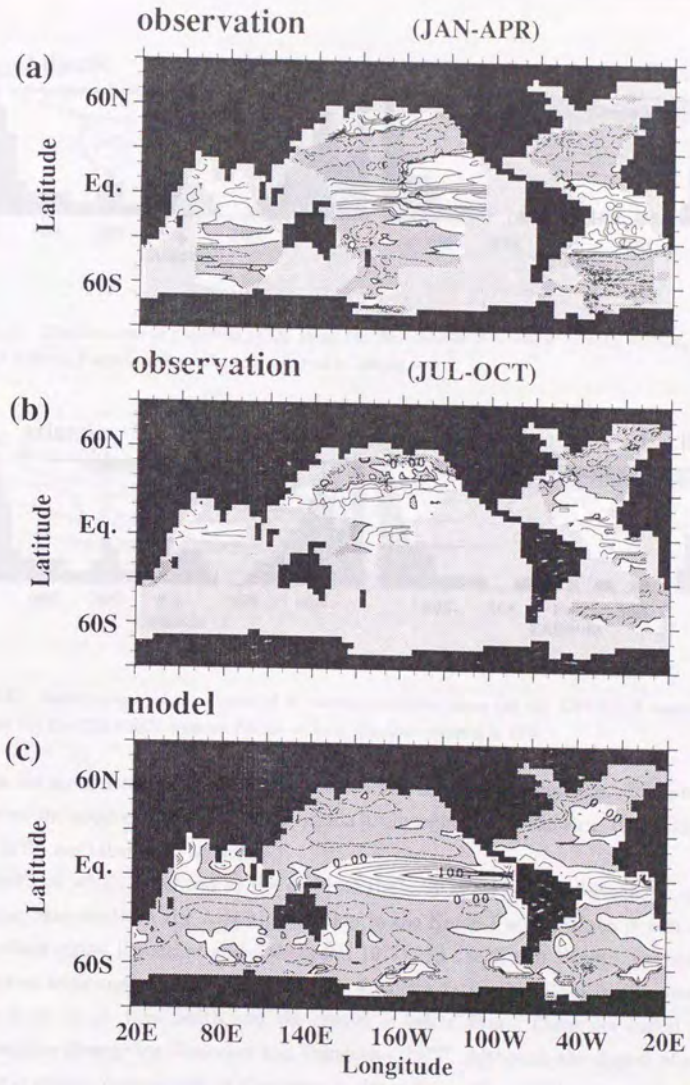

Figure 2-10: Horizontal distribution of ΔpCO_2 from (a) observation (JAN-APR), (b) observation (JUN-OCT), and (c) model result. Observations are after Tans *et al.*[1990]. Contour interval is 20μatm. Light shaded area represents the region without observational data. Dark shaded area represents the region where the oceanic pCO_2 is lower than the atmospheric pCO_2.

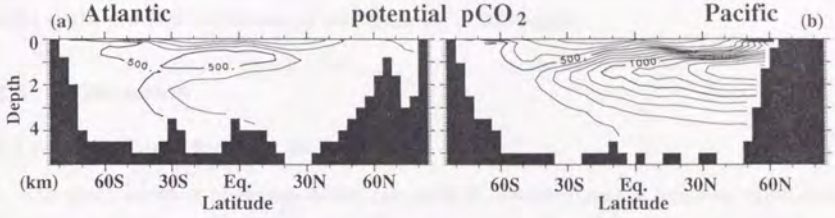

Figure 2-11: Distributions of potential pCO_2 along (a) the GEOSECS western Atlantic section, and (b) the GEOSECS western Pacific section. Contour interval is 100μatm.

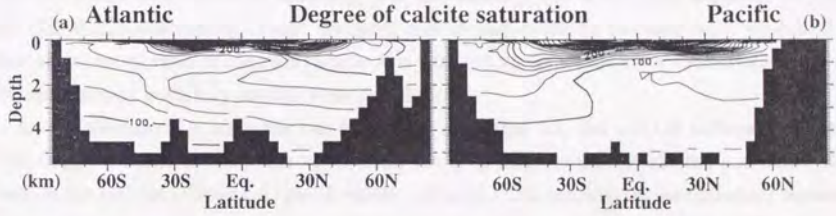

Figure 2-12: Distributions of the degree of of calcite saturation along (a) the GEOSECS western Atlantic section, and (b) the GEOSECS western Pacific section. Contour interval is 10%.

carbonate ion concentration under assumption of the chemical equilibrium. The pressure dependence on the apparent dissociation constants [Culberson and Pytkowicz, 1968; Edmond and Gieskes, 1970] are taken into account.

The lysocline, which is defined as the depth of the saturation horizon for calcite, is found to be at about 5km depth in the Atlantic and 1km in the North Pacific, which is well compared with the observation [Broecker and Takahashi, 1977]. In the North Pacific, we can find the following two minimum regions of the degree of calcite saturation level in the vertical: the shallower is at about 1km depth and the deeper is below 3km. These are called a zone of calcite lysocline divergence [Broecker and Takahashi, 1977]. Although the degree of saturation for calcite is mainly determined by the pressure dependence of solubility, the under-saturation seen at the depth of 1km in the North Pacific is due to the low concentration of carbonate ion in this region. This is because this water mass has contained much carbon owing to an effective

remineralization of POC, and hence the chemical equilibrium ($CO_2 + CO_3^{2-} + H_2O \rightleftharpoons 2\,HCO_3^-$) shifts in the direction of decrease in carbonate ion in this region.

2.5 Discussion

2.5.1 Case Study for Rain Ratio

To study an effect of change in the rain ratio R, we calculate the following three cases: R =0.045 (the control case; Exp.1), 0.12 (Exp.2), and 0.25 (Exp.3).

Figure 2-13 shows the plot of alkalinity against total CO_2 for each water mass in the world ocean. The production rate of calcite which is related to the rain ratio controls alkalinity of each water mass. As clearly seen in this figure, the results of the control case is well compared with the GEOSECS observation of alkalinity. But the results of the other cases are different from the GEOSECS observation. From the other case-studies changing the rain ratio, we consider that the optimal value of the rain ratio is $R = 0.04 \sim 0.06$, as alkalinity of the surface water in the control case is slightly smaller than the observed.

As was discussed by using the two-box model in section 2.3, the ratio of difference in total CO_2 concentrations between the surface and the deep layer to that of alkalinity depends not only on the ratio of production rate of calcite to that of POC, but also on the difference between the average remineralization depth of POC ($L_{\rm POC}$) and that of calcite ($L_{\rm calcite}$). We confirm that the rain ratio depends on the average remineralization depth even for the B-GCM. The optimal value of the rain ratio should be changed according to the presumed profiles of POC flux. For example, the rain ratio of 0.02 is found for $a = -2.0$, and similarly, 0.12 for $a = -0.4$ (see table 1). However, as discussed above, $a = -0.988$ (the control case) with $R = 0.04 \sim 0.06$ is the best fit with the observation.

2.5.2 Case Study for Various Vertical Profiles of POC Flux

We study an effect of change in the prescribed profile of POC flux. We calculate the following nine cases: $a = -0.988$ (control profile; Exp 1,4~8), $a = -2.0$ (shallow profile; Exp.9, 10) and $a = -0.4$ (deep profile; Exp.11). As mentioned in section 2.2, the partial pressure of atmospheric CO_2 depends strongly on the bio-production efficiency r. So the cases changing r for each profile of POC flux are studied. Values of parameters for each case are shown in the Table 1.

Figure 2-14 shows the results of the export production against the concentration of atmospheric CO_2 in each case. In the control case, the export production is estimated to be 10.3

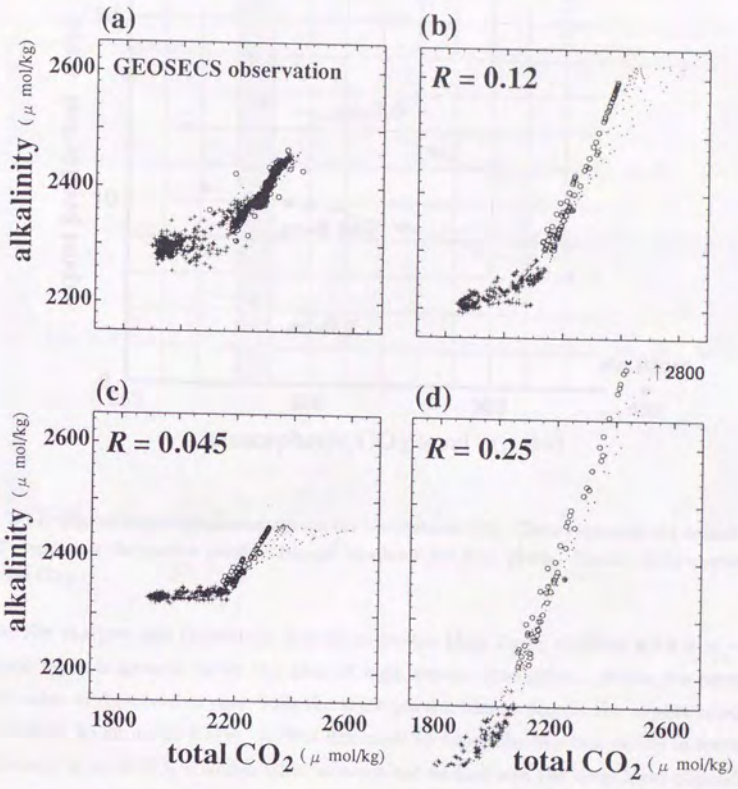

Figure 2-13: Alkalinity and total CO_2 for each water mass in the world ocean: (a) GEOSECS observation; (b) rain ratio R =0.045 (in Exp.1); (c) R =0.12 (in Exp.2); (d) R =0.25 (in Exp.3). Plus represents the surface water (0∼50m deep). Circle represents the deep water (2500∼3000m deep). Dot represents the bottom water (4000∼4500m deep).

GtC/yr, corresponding to the atmospheric CO_2 level of 283 μatm. Because the atmospheric CO_2 reflects the concentration of total CO_2 in the surface water, the atmospheric CO_2 level also represents the global average concentration of total CO_2 in the surface water. With fixed atmospheric CO_2 level at 280 $\sim$ 290μatm (shaded area in Fig.2-14), the export production decreases with an increase in the average remineralization depth. The average remineralization

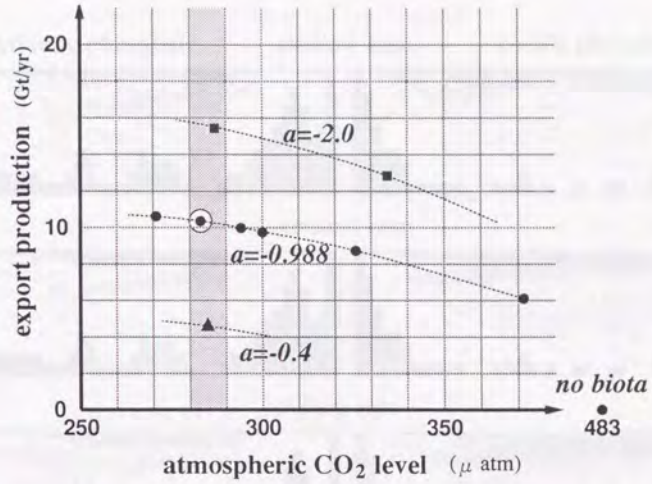

Figure 2-14: Plot of export production against the atmospheric CO_2. Circle represents the control profile. Rectangle represents the shallow profile. Triangle represents the deep profile. Double circle represents the control case (Exp.1).

depth in the shallow case (especially Exp.9) is greater than $L_{POC} = 250$m with $a = -2.0$ as the anoxic layer is formed under the area of high export production. When we permit the negative value of dissolved oxygen with the same parameters as Exp.9, the export production is estimated to be about 20 Gt/yr. As was discussed by using the two-box model in section 2.3, the difference in total CO_2 concentration between the surface and the deep layer depends both on the export production and on the depth where biogenic particulate is remineralized. Although it is not exactly proportional to the average remineralization depth, such a dependence is roughly appropriate for the B-GCM.

Next, we discuss the horizontal distribution of phosphate in the three cases, Exp.1, Exp.9 and Exp.11. In theses cases, the bio-production efficiency is adjusted so as to fit the same concentration of phosphate in the surface water. Figure 2-15 shows the distributions of phosphate along the GEOSECS western Atlantic and western Pacific sections. The phosphate concentration in the North Atlantic decreases with an increase in the average remineralization depth in Figure 2-15(a→c→e). On the other hand, the phosphate concentration in the North Pacific increases with an increase in the average remineralization depth. Horizontal contrast of

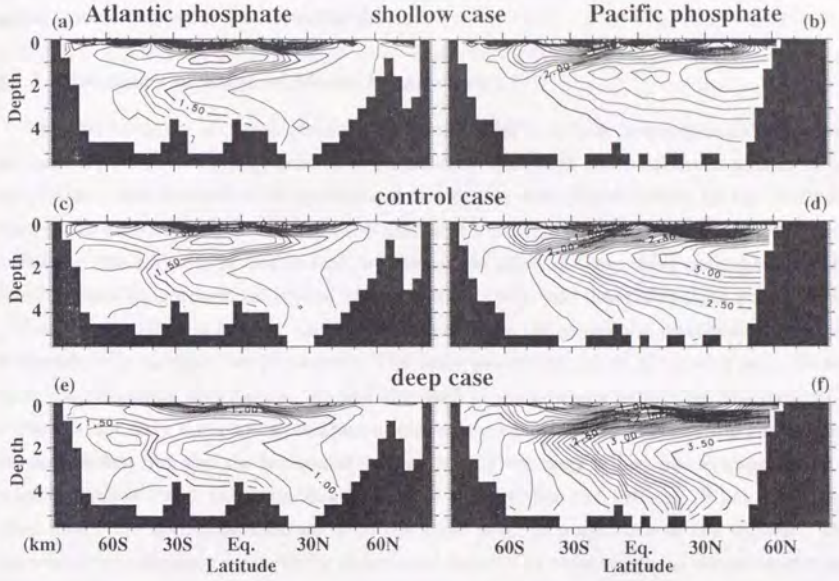

Figure 2-15: Meridional section of phosphate along (a) the GEOSECS western Atlantic in shallow profile case (Exp.9), (b) the GEOSECS western Pacific in shallow profile case (Exp.9), (c) the GEOSECS western Atlantic in control profile case (Exp.1), (d) the GEOSECS western Pacific in control profile case (Exp.1), (e) the GEOSECS western Atlantic in deep profile case (Exp.11), and (f) the GEOSECS western Pacific in deep profile case (Exp.11). Contour interval is 0.1μmol/kg.

phosphate in the deep water also depends on the vertical profile of POC flux. The horizontal contrast increases with an increase in the average remineralization depth. The reason is as follows: although the export production for the deep profile case is smaller than that for the control case, the amount of remineralization of POC in the deep water is larger. Besides the horizontal advective-diffusive flux is dominant in the deep layer. Then, the deep water becomes rich in phosphate due to the remineralization of POC in the course of advection from the North Atlantic to the North Pacific. Therefore, the horizontal contrast of phosphate concentration increases with an increase in average remineralization depth. The horizontal contrast of phosphate in the control case ($a = -0.988$, the observed profile of POC flux by sediment trap) provides the most appropriate result among the three cases. It is noted that the depth of the

phosphate maximum becomes deeper (about the depth of 3km) in the deep profile case as the anoxic layer is formed in the North Pacific.

2.5.3 Summary of Roles of Model Parameters

In order to extend an ocean general circulation model to include biogeochemical processes, we must introduce many biogeochemical parameters. Although these processes appear to be complicated, distributions of biogeochemical tracers are determined mainly by the following three parameters: the exponent of vertical profile of POC flux a, the bio-production efficiency r, and the rain ratio R. In this section, we discuss the effect of these three parameters on the distribution of biogeochemical tracers and the carbon cycle, and determine these parameters.

First, the parameters a and r can be determined from the phosphate distribution, because it depends only on these two parameters. The other parameters, such as the rain ratio, do not affect the phosphate distribution. As was discussed in the previous subsection, the parameter a controls not only the vertical contrast of concentration of tracers between the surface and the deep water, but also the horizontal contrast within the deep water. For example, when a is large (shallow case), the horizontal contrast is smaller than the vertical. When it is small (deep case), the horizontal contrast is on the same order of magnitude as the vertical. The bio-production efficiency r can not be determined directly by observation, as we parameterized biological processes in a very simple way. The results of case-studies for using various r (Exp.1 and Exp.4~Exp.8) show that both the vertical and the horizontal contrasts become stronger with an increase in r while roughly keeping a constant vertical against horizontal contrast ratio. Using the above features of a and r, we can determine the optimal set of these values, as was discussed in the previous subsection. The optimal value of a determined from the phosphate distribution coincides with the value obtained from many observations by using the sediment trap [e.g. Martin *et al.*, 1987; Suess *et al.*, 1980]. This means that the observed value of a can reasonably explain the observed phosphate distribution.

The export production is not determined from the vertical contrast of phosphate concentration between the surface and the deep water, because the vertical contrast depends not only on the export production but also on the average remineralization depth as was discussed in section 2.3 (see equation 2-7). However, the value of export production is automatically determined from the optimal estimates of a and r. The export production consistent with the observed distribution of phosphate is estimated to be about 10 GtC/yr. When DOC is included in our model, it is estimated to be about 9 GtC/yr as will be studied in chapter 3. This value is within the observed estimates which range from $3.4 \sim 7.4$GtC/yr [Eppley, 1989] to 20 GtC/yr

[Packard *et al.*, 1988].

Next, we determine the value of rain ratio R. As the phosphate distribution is determined from a and r, distributions of the other chemical tracers except alkalinity are automatically determined in our model. However, only alkalinity distribution can not be reproduced by using the rain ratio of 0.25, which has been used widely in the previous studies [e.g., Broecker and Peng, 1982]. As was discussed in the previous subsection, we can obtain the rain ratio R from the horizontal/vertical distribution of alkalinity and total CO_2 (Figure 2-13). The value of the rain ratio from our B-GCM study coincides with the value estimated by using our two-box model in section 2.3, which is about 0.04.

In this way, we found the optimal values for three parameters, a, r, and R. With the optimal values of these parameters, the calculated atmospheric CO_2 level is consistent with the observed. The distributions of other chemical tracers, such as dissolved oxygen, total CO_2, and alkalinity, are well compared with the observation only when the optimal parameter values are used in the model.

2.6 Conclusion

The realistic distributions of tracers have been reproduced by using a biogeochemical general circulation model. The depth of the phosphate maximum in the Atlantic and the Pacific is well compared with the observation. The calculated maximum value of phosphate exists in the northern part of the North Pacific, which coincides with the observation.

The difference in the concentrations of tracers between the surface and the deep water depend not only on the export production but also on the average remineralization depth. The classical value of the rain ratio (=0.25) should be modified by taking into account the difference in the average remineralization depths of POC and calcite. When the carbonate sedimentation on the deep sea floor is taken into account, we found that the value of the rain ratio in the real ocean is expected to be 0.06~0.08. The vertical profile of POC flux affects not only the vertical contrast of concentration of tracers between in the surface and the deep water, but also on the horizontal contrast within the deep water. Phosphate distribution can be reproduced only when the profile of POC flux observed by the sediment trap is used. The export production consistent with the observed distribution of phosphate is estimated to be about 10 GtC/yr.

Manabe and Stouffer [1993] suggest that the ocean circulation will drastically change owing to the global warming when the atmospheric CO_2 level becomes four times larger than the present one. In such a case, only a B-GCM can predict the distribution of tracers even when the ocean circulation may change from the present state. How does it affect the carbon cycle

in the ocean? Does the carbon cycle provide a negative feedback mechanism against climate change? We should answer these questions in the future by using the biogeochemical general circulation model.

Acknowledgements

We would like to thank Prof. Nobuo Suginohara for his helpful discussion and encouragements, and also his critical reading of the manuscript. We would also like to thank Prof. Taro Takahashi for his comments and his kindness for giving us his data. Thanks an extended to Dr. Ryuji Tada and the members of paleoclimate colloquium for their helpful discussions and comments. Numerical calculations were performed by HITAC M-3800 at the Computer Center of the University of Tokyo. Figures were produced by GFD-Dennou Libraries on SUN Microsystems SS2.

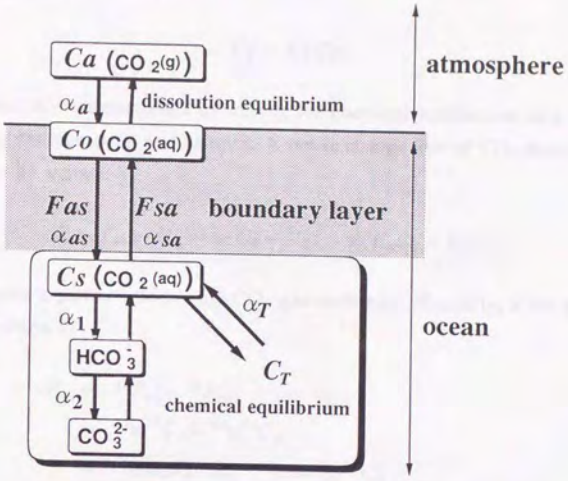

Figure 2-A1: Schematic diagram of gas exchange for CO_2. α represents a fractionation factor of ^{13}C to ^{12}C.

Appendix for Chapter 2 Treatment of ^{13}C in Our Model

In the gas exchange process (Figure 2-A1), gas exchange rate is controlled by diffusion in the boundary layer at the air-sea interface [Broecker and Peng, 1982]. In the following discussion, we assume $^{13}R \equiv {}^{13}C/C \simeq {}^{13}C/{}^{12}C$, which is considered to be a good approximation [Keeling, 1981].

Gas exchange between the atmospheric CO_2 and CO_2(aq) at the top of the boundary layer is faster than diffusion within the boundary layer. Therefore, we can assume a dissolution equilibrium. A relationship between concentration of atmospheric CO_2 ($= C_a$) and that of CO_2(aq) at the top of diffusion layer ($= C_o$) is expressed as,

$$C_o = K_a C_a, \qquad (2 - \mathrm{A1})$$

where K_a represents an apparent solubility constant. In the ocean, CO_2, HCO_3^-, and CO_3^{2-} are in the chemical equilibrium. When the alkalinity, temperature, and salinity are given, concentration of CO_2(aq) at the bottom of the boundary layer ($= C_S$) can be expressed by

concentration of total CO_2 ($= C_T$) as

$$C_S = K_T C_T, \qquad (2-\text{A2})$$

where a coefficient K_T is determined by solving the chemical equilibrium as a function of alkalinity, total CO_2, temperature, and salinity. A net exchange flux of CO_2 from the atmosphere to the ocean can be written as

$$F = F_{as} - F_{sa} = w(C_o - C_S) = w(K_a C_a - K_T C_T), \qquad (2-\text{A3})$$

where w represents a piston velocity for CO_2 gas exchange. Similarly, a net exchange flux of $^{13}CO_2$ can be written as

$$\begin{aligned} F &= {}^{13}F_{as} - {}^{13}F_{sa} \\ &= {}^{13}w\,{}^{13}C_o - {}^{13}w\,{}^{13}C_S \\ &= {}^{13}w\alpha_a K_a\,{}^{13}C_a - {}^{13}w\alpha_T K_T\,{}^{13}C_T \\ &= \alpha_a \frac{{}^{13}w}{w}(wK_aC_a)\frac{{}^{13}C_a}{C_a} - \alpha_T \frac{{}^{13}w}{w}(wK_TC_T)\frac{{}^{13}C_T}{C_T} \\ &\equiv \alpha_{as}F_{as}\,{}^{13}R_a - \alpha_{sa}F_{sa}\,{}^{13}R_T, \end{aligned} \qquad (2\text{-A4})$$

where ${}^{13}w$ is a piston velocity for $^{13}CO_2$ gas exchange, α_a represents a fractionation factor for dissolution equilibrium, α_T represents a fractionation factor for the chemical equilibrium between CO_2, HCO_3^- and CO_3^{2-}, ${}^{13}R_a$ is $^{13}C/^{12}C$ of atmospheric CO_2, and ${}^{13}R_T$ is $^{13}C/^{12}C$ of total CO_2. α_{as} and α_{sa} represent one-way fractionation factors, which are defined as follows:

$$\alpha_{as} \equiv \alpha_a \frac{{}^{13}w}{w}, \qquad (2\text{-A5})$$

$$\alpha_{sa} \equiv \alpha_T \frac{{}^{13}w}{w}. \qquad (2\text{-A6})$$

A relation between the piston velocity ${}^{13}w/w$ and the diffusion coefficient ${}^{13}D/D$ depends on a presumed gas exchange model. For example, it is represented by $w \propto \sqrt{D}$ for the film replacement model, or $w \propto D$ for the stagnant film model [Broecker and Peng, 1982]. A ratio of diffusion coefficient of ^{13}C to ^{12}C is ${}^{13}D/{}^{12}D = 0.9991$ [Schönleber,1976, see Siegenthaler and Münnich, 1981]. According to Siegenthaler and Münnich [1981], we assume that a ratio of

piston velocity of ^{13}C to that of ^{12}C is

$$\frac{^{13}w}{w} = 0.9991. \qquad (2-\text{A7})$$

The temperature dependencies of fractionation factors are

$$\alpha_a = \frac{(^{13}C/^{12}C)_{CO_2(aq)}}{(^{13}C/^{12}C)_{CO_2(g)}} = 0.19 - 0.373\frac{10^3}{T}\ ‰ \qquad (2\text{-A8})$$

$$\alpha_1 = \frac{(^{13}C/^{12}C)_{CO_2(aq)}}{(^{13}C/^{12}C)_{HCO_3^-}} = 24.12 - 9.866\frac{10^3}{T}\ ‰ \qquad (2\text{-A9})$$

$$\alpha_2 = \frac{(^{13}C/^{12}C)_{CO_2(aq)}}{(^{13}C/^{12}C)_{CO_3^{2-}}} = -7.1\ ‰\ , \qquad (2\text{-A10})$$

which are taken from Mook *et al.*[1974] and Siegenthaler and Münnich [1982]. Therefore, α_T is

$$\alpha_T = \frac{[CO_2] + \alpha_1[HCO_3^-] + \alpha_2[CO_3^{2-}]}{[CO_2] + [HCO_3^-] + [CO_3^{2-}]}. \qquad (2-\text{A11})$$

In this way, when alkalinity, temperature, and salinity are given, α_{as} and α_{sa} can be calculated. For example, $\alpha_{as} = -2.01‰$ and $\alpha_{sa} = -10.85‰$ are obtained for the global sea surface average conditions of $T = 13°C$ and $S = 35psu$. The value of fractionation factors agrees with Tans *et al.*[1993]. Similarly, fluxes of $^{13}F_{as}$ and $^{13}F_{as}$ are also calculated under given conditions.

References

Bacastow, R., and E. Maier-Reimer (1990): Ocean-circulation model of the carbon cycle., *Clim. Dynamics*, 4, 95-125.

Bainbridge, A.E. (1981): *GEOSECS Atlantic Expedition*, vol.1., *Hydrographic Data, 1972-1973*, 120pp., U.S. Government Printing Office, Washington, D.C..

Broecker, W.S., and P.-H. Peng (1982): *Tracers in the Sea.*, Lamont-Doherty Geological Observatory, Palisades, New York.

Broecker, W.S., and T. Takahashi (1978): The relationship between lysocline depth and *in situ* carbonate ion concentration., *Deep Sea Res.*, 25, 65-95.

Bryan, F. (1987): Parameter sensitivity of primitive general circulation models., *J. Phys. Oceanogr.*, 17, 970-985.

Bryan, K. (1969): A numerical method for the study of the circulation of the world ocean., *J. Comput. Phys.*, 4, 347-376.

Craig, H., W.S. Broecker, and S. Spenser (1981): *GEOSECS Pacific Expedition*, vol.4., *Hydrographic Data, 1973-1974*, U.S. Government Printing Office, Washington, D.C..

Culberson, C.H., and R.M. Pytkowicz (1968): Effect of pressure on carbon acid, boric acid and the pH in the sea water., *Mar. Chem.*, 1, 295-307.

Dickson, A.G., and F.J. Millero (1987): A comparison of the equilibrium constants for the dissociation of carbonic acid in sea water media., *Deep Sea Res.*, 34, 1733-1743.

Dickson, A.G., and J.P. Riley (1979): The estimation of acid dissociation constants in seawater media from potentiometric titrations with strong base. I. The ionic product of water (K_w)..., *Mar. Chem.*, 7, 89-99.

Edmond, J.M., and J.M. Gieskes (1970): On the calculation of the degree of saturation of sea water with respect to calcium carbonate under *in situ* conditions., *Geochemica cosmochimica acta*, 34, 1261-1291.

England, M.H. (1993): Representing the global-scale water masses in ocean general circulation models., *J. Phys. Oceanogr.*, 23, 1523-1560.

Eppley, R.W. (1989): History, methods, problems., in *Productivity of Ocean: Present and Past*, edited by V.S. Smetacek, G. Wefer and W.H. Berger, pp.85-97, John Wiley, New York.

Johansson, O., and M. Wedborg (1979): On the evaluation of potentiomatric titrations of seawater with hydrochloric acid., *Oceanologica Acta*, 5, 209-218.

Keeling, C.D. (1981): The modeling of rare isotopic carbon with regard to notations., in *Carbon Cycle modeling* In *Scope,* vol.16, edited by B. Bolin, pp.89-94, John Wiley, New York.

Kroopnick, P.M. (1985): The distribution of ^{13}C of ΣCO_2 in the world oceans., *Deep Sea Res.*, 32, 57-84.

Heinze, C., E. Maier-Reimer, and K. Winn (1991): Glacial pCO_2 reduction by the World Ocean: Experiments with the Hamburg carbon cycle model., *Paleoceanogr.*, 6, 395-430.

Hellerman, S., and M. Rosenstein (1983): Normal monthly wind stress over the world ocean with error estimates., *J. Phys. Oceanogr.*, 13, 1093-1104.

Ledwell, J.R., A.J. Watson, and C.S. Law (1993): Evidence for slow mixing across the pycnocline form an open-ocean tracer-release experiment., *Nature*, 364, 701-703.

Levitus, S. (1982): Climatological atlas of the world ocean., *NOAA Prof. Rep. 13*, Natl. Oceanic and Atmos. Admin, Boulder,Colo..

Levitus, S., M.E. Conktight, J.L. Reid, R.G. Najjar, and A. Mantyla (1993): Distribution of nitrate, phosphate and silicate in the world oceans preindustrial tracer distributions., *Prog. Oceanogr.*, 31, 2445-273.

Manabe,S., and R.J. Stouffer (1993): Century-scale effects of increased atmospheric CO_2 on the ocean–atmosphere system., *Nature*, 364, 215-218.

Maier-Reimer, E. (1993): Geochemical cycles in an ocean general circulation model. preindustrial tracer distributions., *Global Biogeochem. Cycles*, 7, 645-677.

Martin, J.H., G.A. Knauer, D.M. Karl, and W.W. Broenkow (1987): VERTEX: Carbon cycling in the northeast Pacific., *Deep Sea Res.*, 34, 267-285.

Mook, W.G., J.C. Bommerson and W.H. Staverman (1974): Carbon isotope fractionation between dissolved bicarbonate and gaseous carbon dioxide., *Earth Planet. Lett.*, 22, 169-176.

Najjar, R.G., J.L. Sarmiento, and J.R. Toggweiler (1992): Downward transport and fate of organic matter in the ocean: Simulations with a general circulation model., *Global Biogeochem. Cycles*, 6, 45-76.

Ostlund, H.G., and M. Stuiver (1980): GEOSECS Pacific radiocarbon., *Radiocarbon*, 22, 25-53.

Packard, T.T., M. Denis, and P.L. Garfield (1988): Deep-ocean metabolic CO_2 production: calculations from ETS activity., *Deep Sea Res.*, 35, 371-382.

Rintoul, S.R. (1991): South Atlantic interbasin exchange., *J. Geophys. Res.*, 96, 2675-2692.

Siegenthaler, U., and K.O. Münnich (1981): $^{13}C/^{12}C$ fractionation during CO_2 transfer from air to sea., in *Carbon Cycle modeling* In *Scope*, vol.16, edited by B. Bolin, pp.249-257, John Wiley, New York.

Stuiver, M., and H.G. Ostlund (1980): GEOSECS Atlantic radiocarbon., *Radiocarbon*, 22, 1-24.

Suess, E. (1980): Particulate organic carbon flux in the oceans — Surface productivity and oxygen utilization., *Nature*, 288, 260-263.

Suginohara, N., S. Aoki, and M. Fukasawa (1990): Comments on "On the importance of vertical resolution in certain oceanic general circulation models"., *J. Phys. Oceanogr.*, 21, 1699-1701.

Sundquist, E.T. (1985): Geological perspectives on carbon dioxide and the carbon cycle., in *The Carbon Cycle and Atmospheric CO_2: Natural Variations Archean to Present*, edited by E.T. Sundquist and W.S. Broecker, pp.5-59, AGU, Washington,D.C..

Toggweiler, J.R., K. Dixon, and K. Bryan (1989): Simulations of Radiocarbon in a Coarse-Resolution World Ocean Model 1. Steady State Prebomb Distributions., *J. Geophys. Res.*, 94, 8217-8242.

Takahashi, T., W.S. Broecker, and Bainbridge (1981): The alkalinity and total carbon dioxide concentration in the World Oceans., in *Carbon Cycle modeling* In *Scope*, vol.16, edited by B. Bolin, pp.271-286, John Wiley, New York.

Takahashi, T., C. Goyet, D.W. Chipman, E. Peltzer, J. Goddard, and P.G. Brewer (1990): Ratio of organic carbon and calcium carbonate productions observed at the JGOFS 47°N-20°W site., (abstract), *JGOFS Rep.,7*, pp.76-77, JGOFS North Atlantic Bloom Experiment International Scientific Symposium, SCOR/ICSU.

Tans, P.P., J.A. Berry, and R.F. Keeling (1993): Oceanic $^{13}C/^{12}C$ Observations: A new window on ocean CO_2 uptake., *Global Biogeochem. Cycles*, 7, 353-368.

Tans, P.P., I.Y. Fung, and T. Takahashi (1990): Observational constraints on the global atmospheric CO_2 budget., *Science*, 247, 1431-1438.

Tsunogai, S., and S. Noriki (1991): Particulate fluxes of carbonate and organic carbon in the ocean. Is the marine biological activity working as a sink of the atmospheric carbon?., *Tellus*, 43B, 256-266.

Weiss, R.F. (1970): The solubility of nitrogen, oxygen and argon in water and sea water., *Deep Sea Res.*, 17, 721-735.

Weiss, R.F. (1974): Carbon dioxide in water and seawater: the solubility of non-ideal gas., *Mar. Chem.*, 2, 203-215.

Chapter 3

Role of Dissolved Organic Carbon in Oceanic Carbon Cycle: Studies Using Ocean Biogeochemical General Circulation Model

Abstract

A biogeochemical general circulation model which includes processes of production and consumption of dissolved organic carbon (DOC) is developed. Semi-refractory and refractory DOC are taken into account. The vertical distribution of DOC concentration and $\Delta^{14}C$ value obtained in our model is well compared with that of the recent observation where the values are determined by the high-temperature combustion method. Is is found that the double DOC maximum zone (DDMZ) extends in the east-west direction in the equatorial Pacific. Case-studies show that the horizontal surface DOC contrast can be reproduced only when the decay time of semi-refractory DOC and the production ratio of semi-refractory DOC against particulate organic carbon (POC) are about (0.5yr,3.0) $\sim$ (1yr,2.0). Semi-refractory DOC exists only above the depth of 400m, and its vertical and horizontal transports play an important role in the oceanic carbon and the nutrient cycles in the surface layer. However, below that depth, only the inert refractory DOC exists and the role of refractory DOC in the carbon cycle is not important. The global export productions due to POC and DOC at the depth of 100m are estimated to be about 9GtC/yr and about 6Gt/yr, respectively. However, the vertical transport below 400m is almost due to POC.

3.1 Introduction

Dissolved organic carbon (DOC) is considered to play an important role in the oceanic carbon cycle. Siegenthaler and Sarmiento [1993] show in their review paper that the flux of DOC transport from the surface to the intermediate and deep layer is about 10 GtC/yr, which is larger than the flux of POC. However, vertical/horizontal distribution of DOC determined by the high-temperature combustion (HTC) method has been reported only for the limited areas [Tanoue, 1993], and its global distribution and flux are not well known.

DOC concentrations determined by the HTC method [Suzuki *et al.*, 1985; Sugimura and Suzuki,1988] were extraordinarily higher than those by the previous methods such as wet chemical oxidation method. Although these reports were withdrawn by Suzuki [1993], the recent observations show that the DOC concentrations determined by HTC method are much lower than those in Sugimura and Suzuki [1988] but still higher than those by the wet chemical oxidation method [Tanoue, 1992; 1993]. Tanoue [1993] showed that DOC concentration in the surface water has a spatial variation of about 80 μmol/kg between the northern North Pacific and the equatorial Pacific. Seasonal variability exists in the surface DOC concentration [Carlson *et al.*, 1994]: DOC accumulates due to spring bloom and is partially consumed in summer and autumn, and it is transported under the euphotic layer by convection in winter. DOC concentration in the deep water is not only vertically but also horizontally uniform from the North Atlantic to the Pacific [Martin and Fitzwater, 1992]. However, comparison of the absolute values of DOC concentration among various observations is difficult, because of errors due to different blank levels between various laboratories [Toggweiler and Orr, 1989; Tanoue, 1993]. $\Delta^{14}C$ values of DOC, $(\Delta^{14}C)_{DOC}$, in the deep North Atlantic and the deep North Pacific are about $-400‰$ and $-520‰$, respectively [Bauer *et al.*, 1992]. Horizontal contrast of $(\Delta^{14}C)_{DOC}$ between the North Atlantic and the North Pacific is the same as that of $\Delta^{14}C$ of dissolved inorganic carbon (DIC). The observed features such as the homogeneous DOC concentration and the horizontal contrast of $(\Delta^{14}C)_{DOC}$ should constrain the DOC behavior in the deep water. That is, most of DOC is transported along with the deep water and it would be conserved.

Previous studies using the biogeochemical general circulation model (BGCM) show that the observed distributions of chemical tracers such as phosphate are reproduced only when DOC is taken into account in their models [Bacastow and Maier-Reimer, 1991; Najjar *et al.*, 1992]. DOC concentrations calculated by them, however, seem to be unrealistically higher than the recent observations. Decay time of their DOC, whose global production rate is about 10GtC/yr, is longer than 50 years, being too long to explain the seasonal variation of DOC. In chapter 2, it was shown that the observed distribution of chemical tracers can be reproduced in BGCM

only when only POC is taken into account. Therefore, the influence of DOC in determining the tracer distributions might be expected to be small. To clarify the roles and behavior of DOC in the oceanic carbon cycle, we need new modeling of DOC based on the recent observations.

Kirchman *et al.*[1993] reported that models dealing with DOC need to consider at least following three pools of DOC: (1) a labile pool with turnover time of days or less, (2) semi-refractory pool with seasonal time scale, and (3) refractory pool with extremely long turnover time (centuries or greater). Although the labile DOC plays an important role in eco-system modeling [*e.g.*, Fasham *et al.*, 1990; Kawamiya *et al.*, 1994], we simply estimate its concentration to be much smaller than 10 μmol/kg whose flux will not affect the global carbon cycle. Therefore, we study the global carbon cycle by using a model in which the semi-refractory DOC and the refractory DOC are taken into account. The Semi-refractory and the refractory DOC will be abbreviated to S-DOC and R-DOC, respectively in this study. Since observation can not distinguish S-DOC from R-DOC, we will not compare individual features of S-DOC and R-DOC obtained in the model with the observed. However, we will explain the observed features of total DOC, the sum of S-DOC and R-DOC, by taking into account these two components of DOC.

In the next section, the model used in this study will be described. In section 3-3, case-studies changing production rate and decay time of S-DOC are made, and horizontal and vertical distributions of S-DOC are discussed. The distribution of R-DOC is also shown. The roles of DOC in the carbon and nutrients cycle will be discussed based on the horizontal and vertical fluxes of DOC. In section 3-4, the results are summarized.

3.2 Model

We developed an ocean biogeochemical general circulation model in Chapter 2, which is basically similar to the model of Bacastow and Maier-Reimer [1990]. The model takes into account processes such as productions and remineralizations of POC and calcium carbonates, air-sea exchanges of $^{12}CO_2$, $^{13}CO_2$ and $^{14}CO_2$, and chemical equilibrium for carbon-related species, which are described in detail in Chapter 2, except the processes of both production and consumption of DOC.

We take into account two types of DOC, the semi-refractory DOC (S-DOC) and the refractory DOC (R-DOC), in this study. Prognostic variables in our model are as follows: the concentrations of atmospheric CO_2, $^{13}CO_2$, $^{14}CO_2$, oceanic total CO_2 (dissolved inorganic carbon, DIC), DI^{13}C, DI^{14}C, alkalinity, phosphate, dissolved oxygen, S-DOC, S-DO^{13}C, S-DO^{14}C, R-DOC, R-DO^{13}C, and R-DO^{14}C.

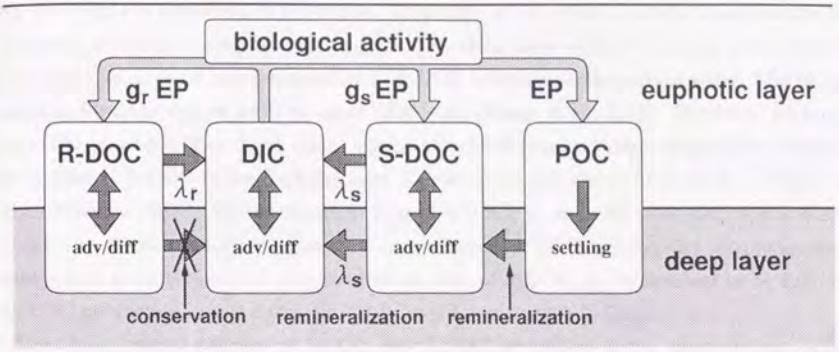

Figure 3-1: Chemical and biological processes included in the B-GCM

The chemical composition of DOC and mechanisms of DOC production and consumption have been little known [Kirchman *et al.*, 1993]. In eco-system modeling, various treatments of DOC production and consumption have been tested [*e.g.*, Fasham *et al.*, 1990; Kawamiya *et al.*, 1994]. Since their treatments are complicated and our purpose is to study the behavior of DOC in global carbon cycle, we treat the DOC production and consumption in the following simple way. Processes concerning DOC in our model are illustrated in Figure 3-1. The production rates of both S-DOC and R-DOC are assumed to be a function of phosphate concentration and light factor, and they are produced at a constant ratio g_s and g_r against that of POC, respectively. g_s is assumed to be $0.5 \sim 4$ (Table 3-1), as production rate of S-DOC is unknown. POC remineralizes into the S-DOC which finally decays to DIC (total CO_2). The decay time of S-DOC, λ_s, is assumed to be $0.25 \sim 20$ years (Table 3-1). The values of $\lambda_s = 0.5 \sim 1.0$ are consistent with the fact that the observed DOC concentrations show the seasonal variations [Carlson *et al.*, 1994]. The $\lambda_s \geq 50$ years used in the previous studies [Bacastow and Maier-Reimer,1991; Najjar *et al.*, 1992] may be inconsistent with the observation.

The important features of DOC behavior obtained from the observation are as fellows: (1) the horizontal contrast of $(\Delta^{14}C)_{DOC}$ between the deep North Atlantic and the deep North Pacific is the same as that of DIC [Bauer *et al.*, 1992], (2) the DOC concentration is horizontally uniform all the way from the deep North Atlantic to the deep Pacific [Martin and Fitzwater, 1992]. These feature indicate that most of DOC is conserved in the deep water; there are no source and sink of DOC in the deep water. Mopper *et al.*[1991] show that photochemical pathway is the rate-limiting step for the decomposition of R-DOC in the sunlit layer above the depth of

5m where light of ultraviolet-B penetrates. Therefore, in this model, R-DOC is assumed to be conserved at depths below the euphotic layer, *i.e.*, decay time of R-DOC in the deep water is assumed to be $\lambda_r \rightarrow \infty$, and consumption of R-DOC is limited to the surface water. The global averaged turnover time of DOC is about 5000 years (Bauer *et al.*, 1992). Combined with the ratio of the euphotic layer depth (50m) against the global averaged depth of sea floor (3700m), decay time of R-DOC in the euphotic layer is estimated to be about 70 years (*i.e.*, 5000yr $\times$ 50m / 3700m = 70yr). We use the decay time of R-DOC, λ_r, to be $65 \sim 80$ years in this study (Table 3-1). From the turnover time and concentration of DOC, the R-DOC production rate is estimated to be 0.3GtC/yr. The production ratio of R-DOC, g_r, is assumed to be 0.03, as the POC production rate is about 10GtC/yr in the control case in Chapter 2.

The advection and diffusion of S-DOC and R-DOC are treated in the same manner as for the other chemical tracers. The parameters and constants for the other processes such as POC production, air-sea gas exchange, and chemical equilibrium are exactly the same as those in the control case in Chapter 2.

We performed 22 experiments with various values of model parameters. Parameters used for each case are listed in Table 3-1. We take into account both S-DOC and R-DOC in Exp.1 (control case) and Exp.2, and only S-DOC in Exp.3~21. Parameters in Exp.7 are taken to be the same as those in the control case, in order to examine the effect of R-DOC. As will be discussed in section 3.3.2, R-DOC will not affect the distribution of other chemical tracers. Exp.22 is the same as the control case in Chapter 2. We obtain the distribution of tracers for each case after carrying out the time integration for the 3000 years, which is considered to be long enough for achieving a steady state.

3.3 Results and Discussions

3.3.1 Distribution of Semi-refractory DOC

Figure 3-2 shows the meridional S-DOC distributions in the control case and the observations [Tanoue, 1992; 1993] along the dashed line in Figure 3-3. Since the observations do not determine the absolute values of S-DOC and R-DOC, we assume the "observed S-DOC" is considered to be the difference in DOC concentration between the surface and the deep water, as all of DOC in the deep water is regarded as R-DOC. This assumption will be verified in the later section. This procedure is to avoid errors caused by different blank levels among the various laboratories [Tanoue, 1993; Toggweiller and Orr, 1993]. Observations show that S-DOC concentration has double maxima at 10°N and 5°S with the minimum at the equator, and de-

Table 3-1: Summary of parameters for numerical experiments in this study. g_s and g_r are the bio-production efficiency ratio of semi-refractory DOC and refractory DOC, respectively, against POC production. λ_s and λ_r are decay time of semi-refractory DOC and refractory DOC (yr), respectively. Exp.1 is the control case. Exp.22 is same as the control case in Chapter 2.

Exp.	semi-refractory DOC		refractory DOC	
	g_s	λ_s	g_r	λ_r
1	3.0	0.5	0.03	65.0
2	3.0	0.5	0.03	80.0
3	4.0	0.3	(not considered)	
4	4.0	0.5	(not considered)	
5	4.0	2.0	(not considered)	
6	3.0	0.25	(not considered)	
7	3.0	0.5	(not considered)	
8	3.0	1.0	(not considered)	
9	3.0	2.0	(not considered)	
10	2.0	1.0	(not considered)	
11	2.0	2.0	(not considered)	
12	2.0	4.0	(not considered)	
13	2.0	10.0	(not considered)	
14	1.0	0.25	(not considered)	
15	1.0	0.5	(not considered)	
16	1.0	1.0	(not considered)	
17	1.0	2.0	(not considered)	
18	1.0	4.0	(not considered)	
19	1.0	10.0	(not considered)	
20	1.0	20.0	(not considered)	
21	0.5	10.0	(not considered)	
22	(not considered)		(not considered)	

creases with increasing latitudes. Although the S-DOC production at the equator is higher than that in other areas, the surface water is diluted with S-DOC-poor water upwelled from the subsurface layer. On the other hand, the S-DOC horizontal convergence causes the high S-DOC concentration there, although the S-DOC production off the equatorial region is lower. The latitude of S-DOC maximum depends on the decay time of S-DOC. The latitude increases with an increase in the decay time λ_s (Fig.3-2): 10°N for $\lambda_s = 0.5$yr (Exp.1 and 7), 15°N for

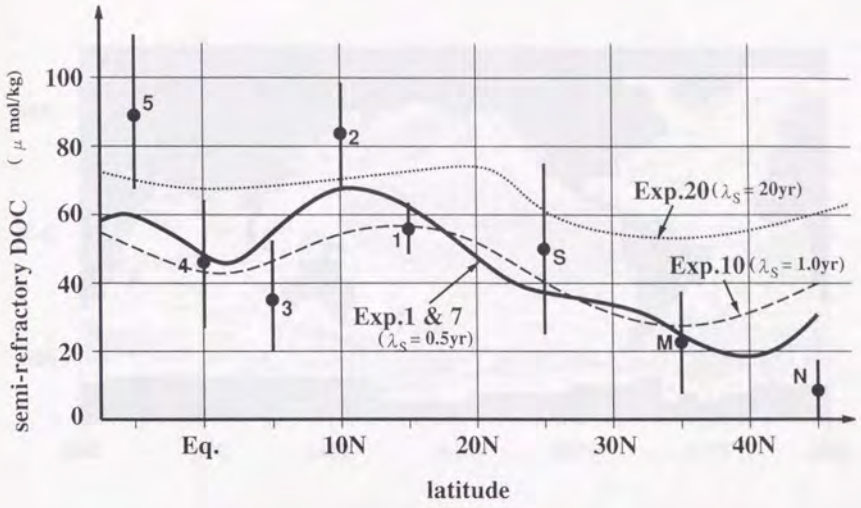

Figure 3-2: Meridional distribution of the difference of semi-refractory DOC concentration between the surface and the deep layer for the model results and for the observations by Tanoue [1992, 1993]. Filled circles are for the observations, marks of 1~5, S, M, and N are the same as observation points in Tanoue [1992, 1993], and error bars are estimated from the deviation in the surface and the deep layer. Thick solid line, thin dashed lines, thin dotted lines are for results in Exp.1 and 7 (control case, λ_s = 0.5yr), Exp.10 (λ_s = 1.0yr), and Exp.20 (λ_s = 20yr), respectively.

λ_s = 2yr (Exp.2), and 20°N for λ_s = 10yr (Exp.20). The latitude of S-DOC maximum in Exp.1 (control case) and Exp.7 is well compared with the observations. The meridional contrast of S-DOC concentration becomes smaller as the decay time increases. The meridional contrast of S-DOC maximum in Exp.1 (control case) and Exp.7 is well compared with the observations, although the contrast is smaller than the observed. The coarse horizontal resolution of our model and effects of computational diffusion yield the smaller contrast.

Figure 3-3 shows the horizontal distribution of S-DOC concentration at the sea surface in Exp.1 (control case). The S-DOC concentration in our model is consistent with the other observations, whose values are 20±12 at M1 in Figure 3-3, 70±12 at M2 [Martin and Fitzwater, 1992], and 14 ± 3 at C [Carlson *et al.*, 1994]. It is found that the double maxima at 10°N and 10°S of S-DOC concentration (Fig.3-3) extend in the east-west direction, i.e., the double DOC maximum zone (DDMZ) exists in the equatorial Pacific. There are regions of low S-

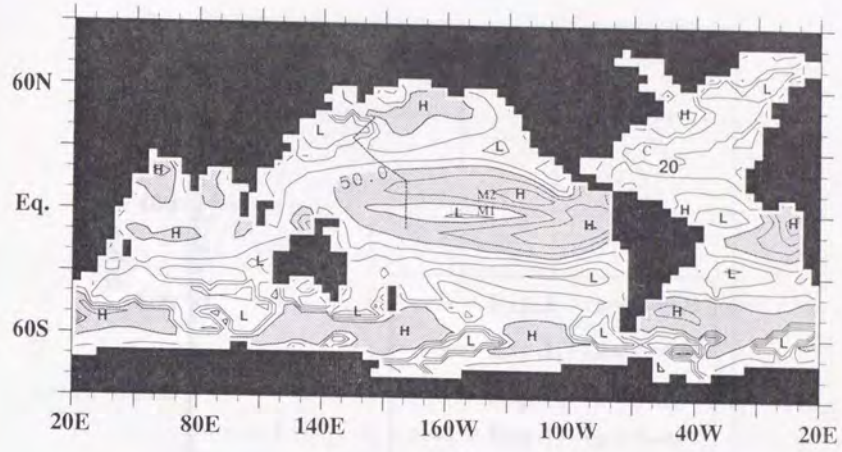

Figure 3-3: Horizontal distribution of the semi-refractory DOC. Dashed line indicates location of meridional line in Figure 3-2. Marks of M1, M2 are the observation points in Martin and Fitzwater [1992]. Mark of C is the observation point in Carlson *et al.*[1994]. Contour intervals = 10μmol/kg.

DOC concentration at high latitudes, where S-DOC is transported to the subsurface layer by convection. The large horizontal contrast of S-DOC concentration at high latitudes is due to the annually averaged condition in our model. This feature may change when we consider the seasonal marching condition.

From the horizontal distribution of S-DOC at the sea surface, we obtain the optimal value of decay time $\lambda_s = 0.5 \sim 1.0$yr. This time scale is much shorter than the horizontal mixing time in the surface water between the high-production and the low-production area. On the other hand, the surface concentration of R-DOC is very uniform because the decay time is longer than the horizontal mixing time in the surface water, as it will be discussed in the next section.

Figure 3-4 shows the vertical S-DOC concentration in the equatorial Pacific in the four cases (Exp.3, Exp.7, Exp.10, and Exp.17), where the surface concentrations are at the common value of about 50 μmol/kg. It is found that S-DOC penetrates into the deeper layer for a longer decay time. The concentration of S-DOC above the depth of 200m in Exp.7 ($\lambda_s = 0.5$yr) and in Exp.10 ($\lambda_s = 1$yr) is higher, whose vertical profiles are well compared with the observation by Tanoue [1993]. In order to objectively compare the calculated vertical profiles of S-DOC with the observed, we consider the surface concentration and the penetration depth of S-

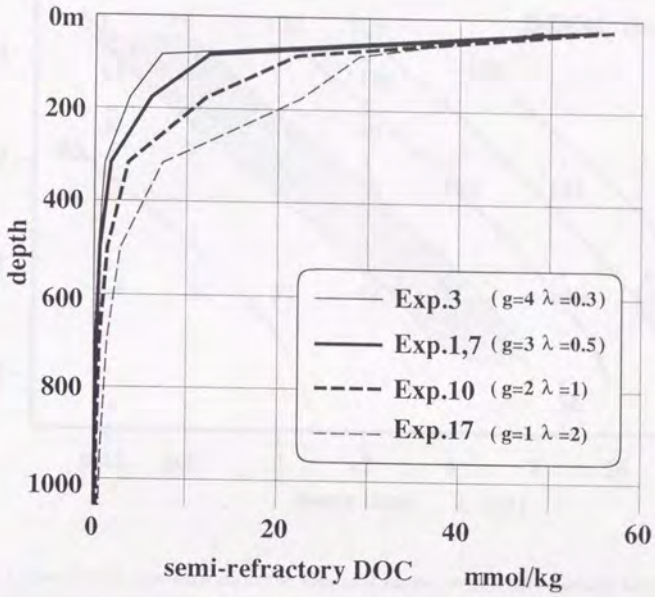

Figure 3-4: Vertical distribution of semi-refractory DOC concentration in the equatorial Pacific (meridionally averaged between 8°S and 8°N along 180°E). Thick solid line is for the control case(Exp.1 and 7). Thick dashed line, thin dashed line, and thin solid line are for Exp.10, Exp.17, and Exp.3, respectively.

DOC in each case. The penetration depth is defined as the vertically integrated concentration divided by the surface concentration. Figure 3-5 shows the equatorial Pacific surface S-DOC concentrations for each case in the S-DOC production ratio – decay time plane. The S-DOC concentration increases with an increase in both the S-DOC production ratio and the decay time. The observed values are about $50 \sim 70 \mu$mol/kg [Tanoue, 1993]. When both the S-DOC production ratio and the decay time are within the range of the shaded area in Figure 3-5, the observed concentration of surface S-DOC is well reproduced. Figure 3-6 shows the globally averaged penetration depth in each case. The penetration depth increases with smaller S-DOC production ratio and with longer decay time. The former is due to maintenance of S-DOC by the decay of POC at depths below the euphotic layer. The penetration depth of S-DOC is close to the vertically averaged remineralization depth of POC when $g_s \rightarrow 0$, as discussed

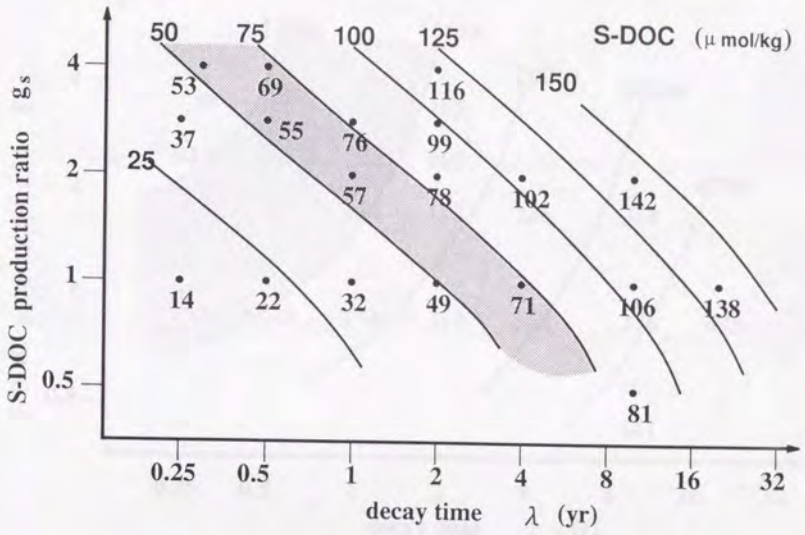

Figure 3-5: Surface S-DOC concentration in the equatorial Pacific (meridionally averaged between 8°S and 8°N along 180°E). Shaded area represents the range where the observation is well reproduced.

in Chapter 2. When the production ratio and the decay time are within the shaded area in Figure 3-5, the observed penetration depth is well reproduced.

From the above discussion on the horizontal and vertical S-DOC distributions, we can constrain the optimal values of the S-DOC production ratio g_s and the decay time λ_s to be $(g_s, \lambda_s) = (3.0, 0.5\text{yr})$ or $(2.0, 1.0\text{yr})$.

3.3.2 Distribution of Refractory DOC

Figure 3-7 shows the R-DOC concentration and its $\Delta^{14}C$ values along the GEOSECS sections in the western Atlantic and the western Pacific. The R-DOC concentration is very uniform, whose value is about 80μmol/kg. When the R-DOC decay time in the surface layer is 80yr, the R-DOC concentration is about 100μmol/kg (Exp.2). Since the observed DOC concentrations in the deep water determined by HTC method range from 80 to 110μmol/kg and the R-DOC concentration is proportional to the R-DOC decay time, the R-DOC decay time is estimated to be 65 $\sim$ 90yr. The production rate of R-DOC in both cases is about 0.3GtC/yr. The

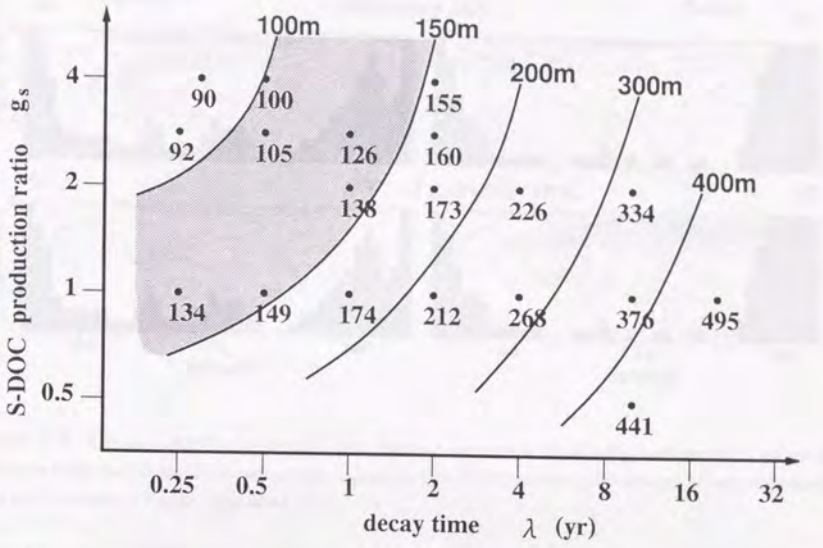

Figure 3-6: Global average penetration depth of S-DOC. Shaded area represents the range where the observation is well reproduced.

turnover time (=R-DOC stock size / production rate) in the surface layer is estimated to be $65 \sim 90$yr, which is equal to the R-DOC decay time in the surface layer. R-DOC concentration is uniform not only in the deep water but also in the surface water, although R-DOC production is horizontally distributed (high-production in the equator region and at high latitudes, low-production in the sub-tropical gyre). The time scale of about 70yr is considered to be longer than the mixing time in the surface water between the high-production and the low-production area.

The distribution of $(\Delta^{14}C)_{\text{R-DOC}}$ is almost similar to that of DIC except that the absolute value of $(\Delta^{14}C)_{\text{R-DOC}}$ is about 300‰ smaller than $(\Delta^{14}C)_{\text{DIC}}$, as the R-DOC is conserved (the difference of 300‰ is due to that of absolute values of $\Delta^{14}C$ between R-DOC and DIC in the surface water). Figure 3-8 shows the vertical profiles of the $(\Delta^{14}C)_{\text{DOC}}$ and $(\Delta^{14}C)_{\text{DIC}}$ in the Sargasso Sea and the North Central Pacific of Bauer *et al.*[1992]. The model results of $(\Delta^{14}C)_{\text{DIC}}$ in the deep North Atlantic and the deep North Pacific are about -240‰ and about -70‰, respectively, which is well compared with the observation. The value of model result

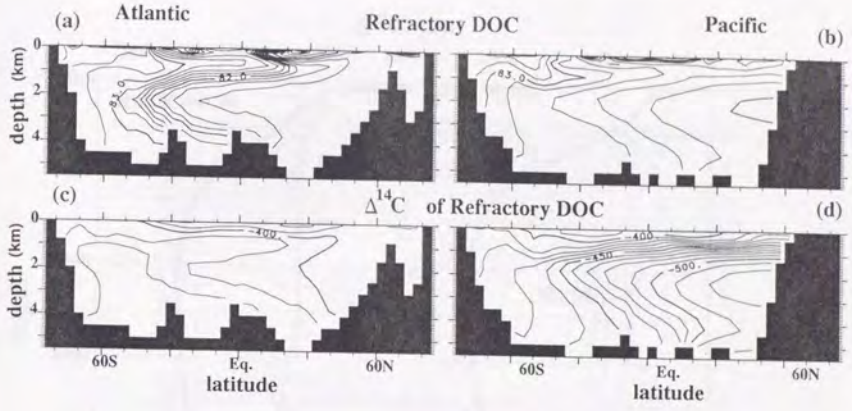

Figure 3-7: Refractory DOC concentration (a,b: Contour intervals is 0.2μmol/kg) and the $\Delta^{14}C$ values of refractory DOC (c,d; Contour intervals is 10‰) along the GEOSECS sections in the western Atlantic (left-hand side) and the western Pacific (right-hand side).

above the depth of 750m is lower than the observed because of the bomb $\Delta^{14}C$ being not taken into account in our model. The model results of $(\Delta^{14}C)_{DOC}$ in the North Atlantic and the North Pacific are about -520‰ and about -400‰, respectively, which are well compared with the observation. The $(\Delta^{14}C)_{DOC}$ in the surface water is about -300‰, which is combination of R-DOC ($(\Delta^{14}C)_{R\text{-}DOC}= -390$‰) with S-DOC ($(\Delta^{14}C)_{S\text{-}DOC}= -80$‰). The value of model result is lower than the observed by about 80‰, because of the bomb $\Delta^{14}C$ being not taken into account. The horizontal contrast of $(\Delta^{14}C)_{DOC}$ between the North Atlantic and the North Pacific ($= 110$‰) is smaller than that of $(\Delta^{14}C)_{DIC}$ ($= 170$‰). However, in the $\Delta^{14}C$ age scale, the horizontal contrast of $(\Delta^{14}C)_{DOC}$ ($= 1800$yr) is slightly larger than that of $(\Delta^{14}C)_{DIC}$ ($= 1700$yr). This is because DIC increases by about 10% due to the remineralization of POC, whose $(\Delta^{14}C)_{POC}$ is about -50‰, but R-DOC is conserved in our model. This means that DOC production in the deep water is well below 10% of the DOC concentration, if any.

The distributions of other chemical tracers in Exp.7 are almost the same as these in Exp.1 (not shown in this paper), which suggests that R-DOC may not play an active role in the carbon cycle. The R-DOC concentration is estimated to be about 100 μmol/kg, and its amount can not be ignored as a carbon stock size in the ocean. However, the R-DOC production and consumption rates are much smaller than the other fluxes such as export production due to POC and S-DOC. R-DOC does not affect the distributions of other chemical tracers.

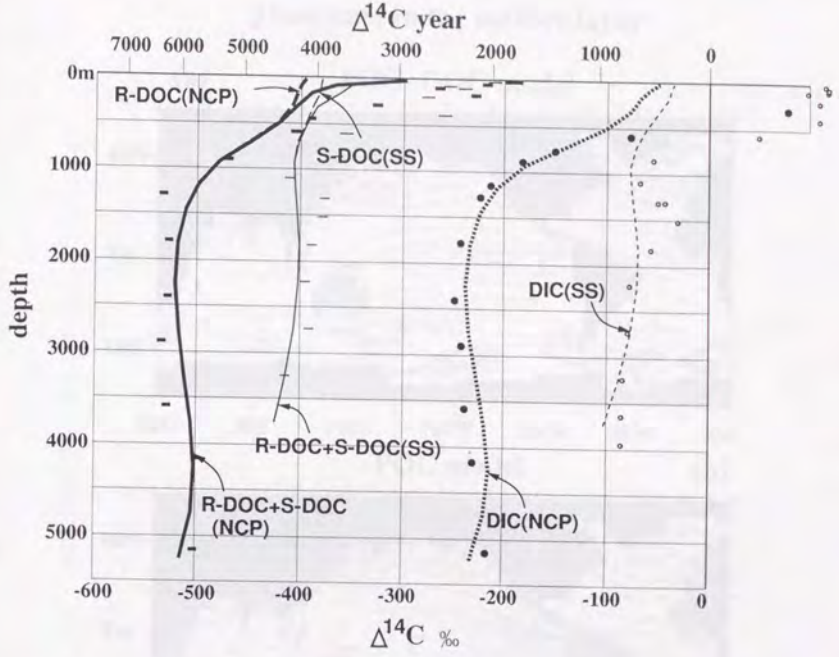

Figure 3-8: Vertical profiles of the $\Delta^{14}C$ values of DOC and DIC. Thick and thin dotted lines are for model results of DIC in the North Central Pacific (32°N,160°W) and the North Atlantic (32°N,64°W), respectively. Thick and thin solid lines are for model results of total DOC which is sum of R-DOC and S-DOC in the North Central Pacific and the North Atlantic, respectively. Thick and thin dashed lines are for model results of R-DOC in the North Central Pacific and the North Atlantic, respectively. Closed circle and thick bar are for observations of DIC and DOC in the North Central Pacific, and open circle and thin bar are for these in the North Atlantic [Druffel *et al.*, 1992].

3.3.3 Role of DOC in carbon cycle

In order to understand the role of DOC in carbon-nutrient cycles, we compare the results such as distribution of phosphate in Exp.1 (DOC is taken into account) with that in Exp.22 (DOC is not taken into account).

Figure 3-9 shows the surface distribution of phosphate concentration in Exp.1 and Exp.22. In both cases, phosphate concentrations at the equator and at high latitudes are higher as the phosphate-rich water is supplied by upwelling and convection. The distribution of surface

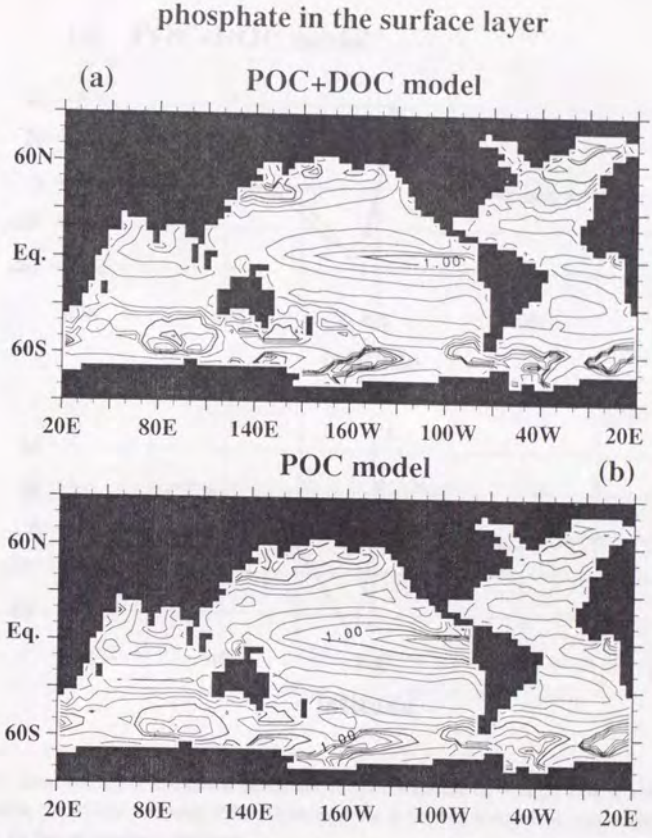

Figure 3-9: Distributions of the phosphate concentration at the surface layer in (a) BGCM with both POC and DOC, and in (b) BGCM with only POC. Contour intervals is 0.2μmol/kg.

phosphate concentration in Exp.1 is compared with the observation better than that in Exp.22. In the subtropical gyre in Exp.1, it is slightly higher than the observed. This may be due to the vertical low-resolution in our model and the calculation under the annually averaged condition.

The maximum values in the high-production areas in Exp.1 are smaller than that in Exp.22. For example, the concentration in the eastern equatorial Pacific is 1.1 μmol/kg in Exp.1 or 1.7μmol/kg. This is because phosphate in the form of dissolved organic phosphate (DOP) is

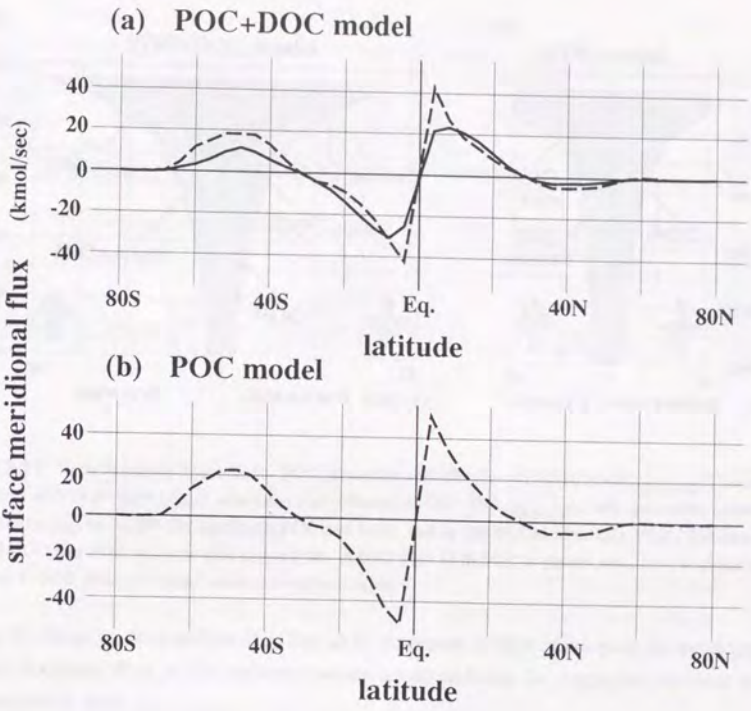

Figure 3-10: Zonal average of meridional phosphate flux in the surface layer in (a) BGCM with both POC and DOC, and in (b) BGCM with only POC. Thick solid line is for flux of dissolved organic phosphate, and thin solid line for flux of inorganic phosphate.

exported from the high-production area by the surface currents such as the Ekman transport, which results in reduction of the "nutrient trapping" of Najjar *et al.*[1992]. Figure 3-10 shows the zonal average of meridional phosphate and DOP transport in the surface layer in Exp.1 and Exp.22. The horizontal transport of DOP in the surface layer is comparable with that of inorganic phosphate as shown in Figure 3-10. The convergence of horizontal DOP transport in the North Atlantic between 24°N and 36°N in Exp.1 is consistent with the estimate by the inverse model [Rintoul and Wunsch, 1991]. The total phosphate transport should be large owing to the DOP transport, as the flux of the inorganic phosphate transport in Exp.1 is

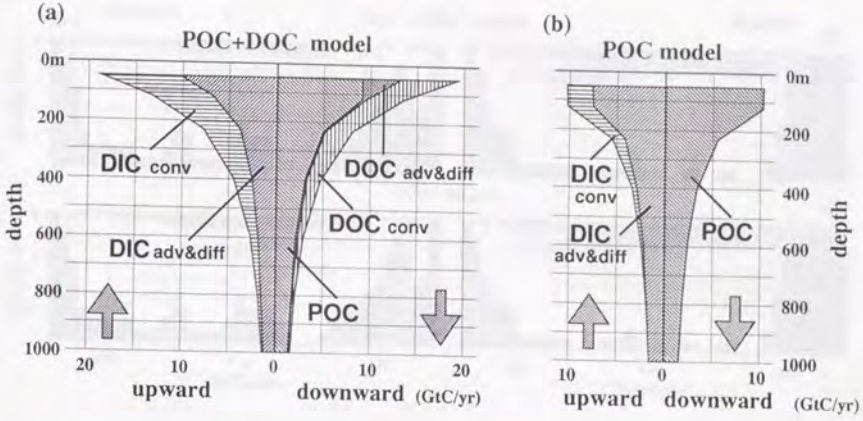

Figure 3-11: Vertical carbon fluxes due to POC, advection and diffusion of S-DOC ($DOC_{adv\&diff}$), convective adjustment of S-DOC (DOC_{conv}), advection and diffusion of DIC ($DIC_{adv\&diff}$), and convective adjustment of DIC (DIC_{conv}) in (a) BGCM with both POC and DOC, and in (b) BGCM with only POC. The downward fluxes of DOC and POC balances with upward flux of DIC. Flux of R-DOC is almost zero, as it is at the steady state and R-DOC does not decay below the euphotic layer.

almost the same as that in Exp.22. The DOP transport is thus important for reducing the nutrient trapping effect in the high-production areas, and also for supplying nutrient to the low-production area.

Figure 3-11 shows the global vertical flux of carbon. Downward fluxes of POC and DOC due to advection/diffusion and convection are balanced with upward fluxes of DIC due to advection/diffusion and convection. Flux of R-DOC is almost zero, as it is almost at the steady state and R-DOC dose not decay below the euphotic layer. The export production, which is defined as the vertical transport of POC at the depth of 100m, is 9GtC/yr in Exp.1. It is slightly smaller than the value of about 10GtC/yr in Exp.22. These results are well within the observed range of $4 \sim 20$GtC/yr [Eppley,1989; Packard *et al.*, 1988]. The export production due to DOC is estimated to be 6GtC/yr. High proportion of the DOC export production is due to S-DOC by the convection, which is consistent with the recent observation [Carlson *et al.*, 1994]. However, the value below the depth of 400m may be overestimated, as the convection in our model is represented by convective adjustment which instantaneously mixes unstably stratified layers. Convection reaching below the depth of 400m is limited to the Greenland

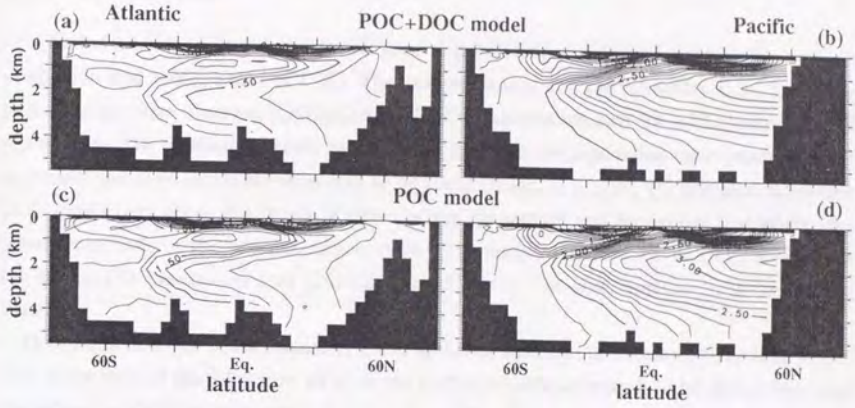

Figure 3-12: Phosphate distributions along the GEOSECS sections in the western Atlantic (left side) and the western Pacific (right side) in BGCM with both POC and DOC, (a,b), and in BGCM with only POC, (c,d). Contour intervals is 0.1μmol/kg.

Sea and the Weddel Sea, and the effect of vertical DOC transport due to convection should be limited to these areas. In other regions, the vertical DOC transport is considered to be limited to the depth above the depth of 400m. Therefore, we can conclude that the important roles of DOC in the vertical carbon transport are restricted above the depth of 400m, and the downward transport below this depth is almost due to POC settling.

Figure 3-12 shows the distributions of phosphate concentration along the GEOSECS sections in the western Atlantic and the western Pacific, which seems to reproduce well the observation. The distributions of phosphate, especially the depth and the value of the phosphate maximum in the Atlantic and the Pacific, are well compared with the observed. The distributions of phosphate in Exp.1 are similar to those in Exp.22. This is because the export production due to POC in the two cases is almost the same (see Figure 3-11) and the downward transport of carbon below the depth of 400m is almost due to POC, i.e., phosphate transport due to DOP downward flux does not play a role in the phosphate cycle below the depth of 400m.

3.4 Conclusion

We have developed a biogeochemical general circulation model which includes processes of production and consumption of DOC. The semi-refractory and the refractory DOC are taken into account. The observed distribution of DOC concentration and its $\Delta^{14}C$ value are well reproduced. The reasonable values for the decay time and the production ratio (against POC) to explain the observation are estimated to be about (0.5yr, 3) $\sim$ (1yr, 2). The semi-refractory DOC exists only above the depth of 400m, where its vertical and horizontal transports play a important role in the oceanic carbon cycle. The surface distribution of DOC shows that the double DOC maximum zone (DDMZ) extends in the east-west direction in the equatorial Pacific.

The production rate of the refractory DOC in the surface layer is estimated to be 0.3GtC/yr. The decay time of the refractory DOC in the surface layer is estimated to be about 70yr, and the refractory DOC is conserved below that layer. From the horizontal contrast of $(\Delta^{14}C)_{DOC}$ between the North Atlantic and the North Pacific, it is estimated that the DOC production in the deep water is well below 10% of the DOC concentration, if any. The role of the refractory DOC in the carbon cycle is not important, because the production and the decay rate of refractory DOC are much smaller than those of semi-refractory DOC and POC, and the refractory DOC does not decay below the surface layer.

The global export production due to POC and DOC at the depth of 100m is about 9GtC/yr and about 6Gt/yr, respectively. However vertical carbon transport below 400m is almost due to POC. The importance of DOC in the carbon cycle would significantly change at the depths between 100m and 400m. Intensive observation of DOC at these depths is required for further understanding roles of DOC in the oceanic carbon cycle.

Acknowledgements

We would like to thank Prof. Nobuo Suginohara for his helpful discussion and encouragements. We would also like to thank Drs. M. Kishi at Ocean Research Institute, University of Tokyo, E. Tanoue at Meteorological Research Institute, and Mr. M. Kawamiya for their helpful discussions and comments.

Numerical calculations were performed by HITAC M-3800 at the Computer Center of the University of Tokyo. Figures were produced by GFD-Dennou Libraries on SUN Microsystems SS2.

References

Bacastow, R., and E. Maier-Reimer (1990): Ocean-circulation model of the carbon cycle., *Clim. Dynamics*, 4, 95-125.

Bacastow, R., and E. Maier-Reimer (1991): Dissolved organic carbon in modeling oceanic new production., *Global Biogeochem. Cycles*, 5, 71-85.

Bauer, J.E., P.M. Williams, and E.R.M. Druffel (1992): ^{14}C activity of dissolved organic carbon fractions in the north-central Pacific and Sargasso Sea., *Nature*, 357, 667-670.

Carlson, C.A., H.W. Ducklow, and A.F. Michaels (1994): Annual flux of dissolved organic carbon from the euphotic zone in the northwestern Sargasso Sea., *Nature*, 371, 405-408.

Druffel, E.R.M., P.M. Williams, J.E. Bauer, and J.R. Ertel (1992): Cycling of Dissolved and Particulate Organic Matter in the Open Ocean., *J. Geophys. Res.*, 97, 15639-15659.

Eppley, R.W.(1989): History, methods, problems., In *Productivity of Ocean: Present and Past*, edited by V.S. Smetacek, G. Wefer and W.H. Berger, pp.85-97., New York, John Wiley.

Facham, M.J.R., H.W. Ducklow, and S.M. NcKelvie (1990): A nitrogen-based model of plankton dynamics in the oceanic mixed layer., *J. Mar. Res.*, 48, 591-639.

Kawamiya, M., M. Kishi, Y. Yamanaka, and N. Suginohara (1994): An ecological-physical coupled model applied to Station Papa., *J. Oceanog.*, (submitted).

Kirchman, D.L., C. Lancelot, M. Fasham, L. Legendre, G. Radach, and M. Scott(1993): Dissoled organic matter in biogeochemical models of the ocean., In *Towards a Model of Ocean Biogeohcemical Processes*, NATO ASI Series Vol. I 10, Edited by G.T. Ecans and M.J.R. Facham, pp.209-225., Springer, Berlin.

Martin, J.H., and S.E. Fitzwater (1992): Dissolved organic carbon in the Atlantic, Southern and Pacific oceans., *Nature*, 356, 699-700.

Mopper, K., X. Zhou, R.J. Kieber, D.J. Kieber, R.J. Sikorski, and R.D. Jones (1991): Photochemical degradation of dissolved organic carbon and its impact on the oceanic carbon cycle., *Nature*, 353, 60-62.

Najjar, R.G., J.L. Sarmiento, and J.R. Toggweiler (1992): Downward transport and fate of organic matter in the ocean: Simulations with a general circulation model., *Global Biogeochem. Cycles*, 6, 45-76.

Packard, T.T., M. Denis, and P.L. Garfield (1988): Deep-Ocean metabolic CO_2 production: calculations from ETS activity., *Deep Sea Res.*, 35, 371-382.

Rintoul, S.R., and C. Wunsch (1991): Mass heat oxygen and nutrient fluxes and budgets in the North Atlantic Ocean., *Deep Sea Res.*, 38, Suppl. 1, S355-S377.

Siegenthaler, U., and J.L. Sarmiento (1993): Atmospheric carbon dioxide and the ocean., *Nature*, 365, 119-125.

Sugimura, Y., and Y. Suzuki (1988): A high-temperature catallytic oxidation methods for determination of nonvolatile dissolved organic carbon in seawater by direct injection of a liquid sample., *Mar. Chem.*, 24, 105-131.

Suzuki, Y. (1993): On the measurement of DOC and DON in seeawater., *Mar. Chem.*, 41, 287-288.

Suzuki, Y., Y. Sugimura, and T. Itoh (1985): A catalytic oxidation method for the determination of total nitrogen dissolved in seater., *Mar. Chem.*, 16, 83-97.

Tanoue, E. (1992): Vertical distribution of dissolved organic carbon in the North Pacific as determined by the high-temperature catalytic oxidation method., *Earth Planet. Sci. Lett.*, 111, 201-216.

Tanoue, E. (1993): Distributional characteristics of DOC in the central equatorial Pacific., *J. Oceanog.*, 49, 625-636.

Toggweiler, J.R., and J. Orr(1993): Summary of warkshop on dissolved organic carbon in the ocean., In *The Global Carbon Cycle*, Edited by M. Heimann, pp.584-585., Springer, Berlin.

Chapter 4

General Conclusion

Two types of an ocean biogeochemical general circulation model (B-GCM) have been developed: one takes into account only POC, and the other both POC and DOC. Two components of DOC the semi-refractory DOC and the refractory DOC, are considered.

The phosphate distribution is determined by the following two parameters for production and consumption of POC: the bio-production efficiency r and the exponent of vertical profile of POC flux a. The optimal set of these values can be determined by using the dependency of the phosphate distribution on a and r. The optimal value of a coincides with the value observed by many sediment traps. Thus, the phosphate distribution can be reproduced only when the vertical profile of POC flux observed by the sediment traps is adopted. The widely used value of the rain ratio (=0.25) should be modified by taking into account the difference in the average remineralization depths of POC and calcite. It is found that the value of the rain ratio in the real ocean is 0.06~0.08 when the carbonate sedimentation is included.

The role of DOC in the nutrient and carbon cycles is studied. It is found that the distributions of chemical tracers are determined mainly by the vertical POC flux and ocean circulation. The vertical and horizontal DOC fluxes only affect the distribution of the chemical tracers above the depth of 400m. Below that depth, only the inert refractory DOC exists, and the DOC fluxes do not affect these distributions, because the consumption rate of refractory DOC is much smaller than that of POC. The export production due to POC consistent with the observed distribution of phosphate is estimated to be about 9GtC/yr, whose value is within the estimates based on the observation. The global export production due to DOC at the depth of 100m is about 6Gt/yr, most of which is transported by the convection. However, most of DOC is consumed above the depth of 400m, and the downward nutrients and carbon transports below that depth are almost due to POC.

The case-studies changing the decay time and the production rate of semi-refractory DOC show that the reasonable set to explain the observation is estimated to be (0.5yr, 27GtC/yr) ~ (1yr, 18GtC/yr). The set for the refractory DOC in the surface layer is estimated to be about 0.3GtC/yr and 70yr. The production and consumption of the refractory DOC in the deep layer is estimated to be well below 10% of the DOC concentration, if any.

The dependency of the distribution of chemical tracers on these parameters is clarified, and the observed distributions of chemical tracers, such as phosphate and oxygen, are well reproduced. For example, the depth of the phosphate maximum in the Atlantic and the Pacific is well compared with the observation. The maximum value of the phosphate concentration exists in the northern part of the North Pacific, which coincides with the observation. The DOC distribution in the surface layer shows that the double DOC maximum zone (DDMZ) extends in the east-west direction in the equatorial Pacific. The observed distribution of $(\Delta^{14}C)_{DOC}$

and $(\Delta^{14}C)_{DIC}$ in the deep North Pacific and the deep North Atlantic are well reproduced.

The observed distributions of chemical tracers on the ocean scale are reproduced by taking into account the very simple biological process, whose parameter r is assumed to be a global constant in the world ocean. This indicates that the complication of the marine biological system does not seriously affects the distributions of chemical tracers on the ocean scale. The global production of calcite is estimated to be about 0.5GtC/yr, which is much smaller than that of >2GtC/yr in the previous studies. The calcite sedimentation is estimated to be about 0.2GtC/yr. Since the river input and sedimentation are not at the same place, the transport between these places may affect the distribution of chemical tracers like alkalinity. In order to discuss this problem, improvement of B-GCM, for example, inclusion of the river input and sedimentation processes, is needed. The phosphate budget in the model shows that the high productive region in the equatorial Pacific causes the apparently closed cycling system of phosphate in the Pacific. In order to confirm this ocean-scale nutrient trapping, an intensive study is required.

The biogeochemical general circulation model will be able to predict the distribution of tracers even when the ocean circulation may change from the present state. The effect of changing ocean circulation on the nutrient and carbon cycles need to be clarified in near future.

Appendix A

Chemical Reactions in Biogeochemical General Circulation Model

A.1 Chemical Reactions in Our Biogeochemical General Circulation Model

In this appendix, chemical reactions in B-GCM are described, as details of calculation and dissociation constants among the previous studies and our study are slightly different one another.

A.1.1 Reactions related to carbon dioxide

In order to calculate pCO_2 by using a set of temperature, salinity, total alkalinity, and total carbon dioxide, we consider the carbon-borate-water system. This composes of the following series of chemical equilibrium:

$$CO_2(g) \rightleftharpoons CO_2^*, \tag{A-1}$$
$$CO_2^* + H_2O \rightleftharpoons H^+ + HCO_3^-, \tag{A-2}$$
$$HCO_3^- \rightleftharpoons H^+ + CO_3^{2-}, \tag{A-3}$$
$$B(OH)_3 + H_2O \rightleftharpoons H^+ + B(OH)_4^-, \tag{A-4}$$
$$H_2O \rightleftharpoons H^+ + OH^-, \tag{A-5}$$

where CO_2^* is the sum of CO_2(aq) and H_2CO_3, as these are difficult to distinguish by analytical means.

A.1.2 Mass and charge balances

Total alkalinity A_T and total carbon dioxide C_T are calculated as prognostic variables determined by the processes in our model such as advection and diffusion. Total borate is a function of salinity. These are defined as follows:

$$A_T \equiv 2[CO_3^{2-}] + [HCO_3^-] + [B(OH)_4^-] + [OH^-] - [H^+], \tag{A-6}$$
$$C_T \equiv [CO_3^{2-}] + [HCO_3^-] + [CO_2^*], \tag{A-7}$$
$$B_T \equiv [B(OH)_4^-] + [B(OH)_3]. \tag{A-8}$$

Apparent dissociation constants in (A-1) through (A-5) are the following functions of temperature and salinity determined by the experimental data as described below,

$$K_0 \equiv \frac{[CO_2^*]}{[CO_2(g)]}, \tag{A-9}$$

$$K_1 \equiv \frac{[H^+][HCO_3^-]}{[CO_2^*]}, \tag{A-10}$$

$$K_2 \equiv \frac{[H^+][CO_3^{2-}]}{[HCO_3^-]}, \tag{A-11}$$

$$K_B \equiv \frac{[H^+][B(OH)_4^-]}{[B(OH)_3]}, \tag{A-12}$$

$$K_W \equiv [H^+][OH^-]. \tag{A-13}$$

The eight concentrations, $[CO_2^*]$, $[CO_2(g)]$, $[H^+]$, $[HCO_3^-]$, $[CO_3^{2-}]$, $[B(OH)_3]$, $[B(OH)_4^-]$, and $[OH^-]$, are determined by a set of eight equations, (A-6) through (A-13).

A.1.3 Solution Method of pCO_2

The variable a is defined as follows:

$$a \equiv \frac{1}{[H^+]}. \tag{A-14}$$

From (A-7), (A-10), and (A-11), the concentrations of carbon dioxide, bicarbonate ion, and carbonate ion can be written as the following functions of a and C_T,

$$[CO_2^*] = \frac{1}{1 + aK_1 + a^2K_1K_2} C_T, \tag{A-15}$$

$$[HCO_3^-] = \frac{aK_1}{1 + aK_1 + a^2K_1K_2} C_T, \tag{A-16}$$

$$[CO_3^{2-}] = \frac{a^2K_1K_2}{1 + aK_1 + a^2K_1K_2} C_T. \tag{A-17}$$

From (A-8), (A-12), and (A-13), the concentrations of borate ion and hydroxide ion can be written as the following functions of a and B_T, respectively,

$$[B(OH)_3] = \frac{1}{1 + aK_B} B_T, \tag{A-18}$$

$$[B(OH)_4^-] = \frac{aK_B}{1 + aK_B} B_T, \tag{A-19}$$

$$[OH^-] = aK_W. \tag{A-20}$$

These equations are substituted into (A-6), and the following equation is obtained,

$$A_T = \frac{2a^2K_1K_2C_T}{1 + aK_1 + a^2K_1K_2} + \frac{aK_1C_T}{1 + aK_1 + a^2K_1K_2} + \frac{aK_BB_T}{1 + aK_B} + aK_W - \frac{1}{a}. \tag{A-21}$$

This is an equation for a, as A_T, C_T, B_T, K_1, K_2, K_B, and K_W are given. The solution of a is obtained from this equation, but is not obtained by analytic method.

We practically solve (A-21) by using the iterative method, as total alkalinity can be approximated to be carbonate alkalinity defined as

$$A_C \equiv 2[CO_3^{2-}] + [HCO_3^-] \tag{A-22}$$

$$= \frac{2a^2K_1K_2C_T + aK_1C_T}{1 + aK_1 + a^2K_1K_2}. \tag{A-23}$$

Its relation to total alkalinity is

$$A_C = A_T - [B(OH)_4^-] - [OH^-] + [H^+] \tag{A-24}$$

$$= A_T - \frac{aK_BB_T}{1 + aK_B} - \left(aK_W - \frac{1}{a}\right). \tag{A-25}$$

If $a^{(1)}$ is given as a suitable first guess, $A_C^{(1)}$ is determined by (A-25). An improved $a^{(2)}$ can be estimated with (A-23) from this value of $A_C^{(1)}$. This iteration procedure of (A-25) and (A-23) yields a suitable n-th guess $a^{(n)}$ which is of convergence, and this value becomes a solution of (A-21).

(A-23) is simplified to be the following quadratic equation with a dimensionless constant $\gamma \equiv A_C/C_T$,

$$(2 - \gamma)K_1K_2a^2 + (1 - \gamma)K_1a - \gamma = 0. \tag{A - 26}$$

Since $\gamma \sim 1.1$ in the real ocean, the solution of (A-26) is

$$a = \frac{-(1 - \gamma)K_1 + \sqrt{(1 - \gamma)^2K_1^2 + 4(2 - \gamma)K_1K_2\gamma}}{2(2 - \gamma)K_1K_2}. \tag{A - 27}$$

Using a determined by the operation above, we determine the other seven concentrations in (A-9) and (A-14) through (A-20).

A.1.4 Apparent dissociation constants

The measurement of apparent dissociation constants is based on several pH scales, such as NBS pH scale (national bureau of standards) and SWS pH scale (sea water scale). These scales are related by the following expression which uses the apparent total hydrogen ion activity coefficient f_H,

$$[H^+]_{NBS} = f_H[H^+]_{SWS}, \tag{A-28}$$

Table A-1: Value of each dissolution constant in prescribed temperature (℃) and salinity (psu)

T	S	K_0	K_1	K_2	K_B	K_W	f_H
0.0	35.0	6.28458×10^{-2}	7.77753×10^{-7}	4.31894×10^{-10}	1.18413×10^{-9}	5.23584×10^{-15}	0.801015
10.0	35.0	4.38649×10^{-2}	1.00871×10^{-6}	6.53286×10^{-10}	1.60927×10^{-9}	1.45834×10^{-14}	0.762485
13.0	35.0	3.98281×10^{-2}	1.08564×10^{-6}	7.35969×10^{-10}	1.75704×10^{-9}	1.95550×10^{-14}	0.750926
20.0	35.0	3.23985×10^{-2}	1.27916×10^{-6}	9.63861×10^{-10}	2.14174×10^{-9}	3.78775×10^{-14}	0.723954
30.0	35.0	2.51656×10^{-2}	1.58980×10^{-6}	1.39038×10^{-09}	2.79716×10^{-9}	9.23756×10^{-14}	0.685424
13.0	33.0	4.02816×10^{-2}	1.06850×10^{-6}	7.07995×10^{-10}	1.71673×10^{-9}	1.88412×10^{-14}	0.745964
13.0	37.0	3.93798×10^{-2}	1.10158×10^{-6}	7.62062×10^{-10}	1.79321×10^{-9}	2.02745×10^{-14}	0.756179

$$[\mathrm{H^+}]_{\mathrm{NBS}} = 10^{-\mathrm{pH(NBS)}}, \tag{A-29}$$

$$[\mathrm{H^+}]_{\mathrm{SWS}} = 10^{-\mathrm{pH(SWS)}}. \tag{A-30}$$

We used SWS pH scale in our model and the below discussion. T is absolute temperature (K), S salinity (psu), and ln natural logarithm.

The solubility of carbon dioxide in seawater $K_0 \equiv [\mathrm{CO_2^*}]/[\mathrm{CO_2}(g)]$ is computed by using the following expression given by Weiss [1974],

$$\begin{aligned} \ln K_0 &= 93.4517\left(\frac{100}{T}\right) - 60.2409 + 23.3585\ln\left(\frac{T}{100}\right) \\ &+ S\left\{0.023517 - 0.023656\left(\frac{T}{100}\right) + 0.0047036\left(\frac{T}{100}\right)^2\right\}. \end{aligned} \tag{A-31}$$

The apparent dissociation constants for carbonic acid, which are defined by

$$K_1 \equiv [\mathrm{H^+}]_{\mathrm{SWS}}[\mathrm{HCO_3^-}]/[\mathrm{CO_2^*}], \quad K_2 \equiv [\mathrm{H^+}]_{\mathrm{SWS}}[\mathrm{CO_3^{2-}}]/[\mathrm{HCO_3^-}],$$

are computed using the following expressions given by Dickson and Millero [1987],

$$\begin{aligned} pK_1 &= 6320.18\frac{1}{T} - 126.3405 + 19.568\ln T \\ &+ \left(19.894 - 840.39\frac{1}{T} - 3.0189\ln T\right)\sqrt{S} + 0.00678S, \end{aligned} \tag{A-32}$$

$$\begin{aligned} pK_2 &= 5143.69\frac{1}{T} - 90.1833 + 14.613\ln T \\ &+ \left(17.176 - 690.59\frac{1}{T} - 2.6719\ln T\right)\sqrt{S} + 0.02169S. \end{aligned} \tag{A-33}$$

where $K_1 = 10^{-pK_1}$ and $K_2 = 10^{-pK_2}$.

The apparent dissociation constant for boric acid, which is defined by

$$K_B \equiv [H^+]_{SWS}[B(OH)_4^-]/[B(OH)_3],$$

is computed using the following expressions given by Johansson and Wedborg [1982],

$$pK_B = 1030.5\frac{1}{T} + 5.5076 - 0.015469S + 1.5339 \cdot 10^{-4}S^2, \qquad (A-34)$$

where $K_B = 10^{-pK_B}$.

The apparent dissociation constants of water, which is defined by $K_W \equiv [H^+]_{SWS}[OH^-]$, is computed using the following expressions given by Dickson and Riley [1979],

$$pK_W = 3441.0\frac{1}{T} + 2.241 - 0.09415S^2 \qquad (A-35)$$

where$K_W = 10^{-pK_W}$.

Total borate concentration is computed as the following function of salinity by Uppstrom [1974].

$$B_T = \frac{0.000232}{10.81}\frac{S}{1.80655}. \qquad (A-36)$$

The set of K_0, K_1,K_2, K_B, K_W, and B_T above is described by DOE [1991].

The apparent total hydrogen ion activity coefficient f_H, which is a value of Culberson and Pytkowicz [1973] by Takahashi *et al.* [1982], is computed using the following expressions,

$$f_H = 1.29 - 0.00204T + 4.6 \times 10^{-4}S^2 - 1.48 \times 10^{-6}S^2T. \qquad (A-37)$$

However, f_H is not used in B-GCM.

The example of each dissolution constant values in prescribed temperature and salinity are shown Table A-1.

A.1.5 Example of calculation

Examples of each concentration obtained by using the calculation in A.1.2 from prescribed temperature, salinity, total alkalinity, and total carbon dioxide are shown in Figures A-1∼5.

Acknowledgments

We thank Dr. Masao Ishii for his helpful imformation about DOE (1991).

Table A-2: Examples of concentration of carbonate alkalinity (A_C) · borate alkalinity (A_B), water alkalinity (A_W), carbon dioxide ([CO_2]), bicarbonate ion ([HCO_3^-]), carbon dioxide ([CO_3^{2-}]), and partial pressure of carbon dioxide calculated from the total alkalinity (A_T), total carbon dioxide (C_T), temperature (T), and salinity (S). Units of temperature, salinity, carbon dioxide partial pressure, and others are ℃, psu, μatm, μmol/kg, respectively.

A_T	C_T	T	S	[H^+]sws	A_C	A_B	A_W	[CO_2]	[HCO_3^-]	[CO_3^{2-}]	pCO_2
2300.	2000.	0.	35.	3.72579×10^{-9}	2198.32	100.28	1.40	8.55	1784.58	206.87	136.03
2300.	2000.	10.	35.	5.46777×10^{-9}	2202.79	94.55	2.66	9.64	1777.94	212.43	219.71
2300.	2000.	13.	35.	6.10992×10^{-9}	2203.94	92.87	3.19	10.00	1776.07	213.94	250.97
2300.	2000.	20.	35.	7.86667×10^{-9}	2206.21	88.98	4.81	10.90	1771.99	217.11	336.36
2300.	2000.	30.	35.	1.11359×10^{-8}	2208.24	83.47	8.28	12.38	1767.00	220.62	491.83
2400.	2000.	13.	35.	4.42290×10^{-9}	2277.37	118.22	4.42	6.96	1708.71	284.33	174.78
2330.	2050.	13.	35.	6.69341×10^{-9}	2240.63	86.45	2.92	11.32	1836.72	201.96	284.33
2300.	2100.	13.	35.	9.49134×10^{-9}	2233.00	64.95	2.05	16.90	1933.20	149.90	424.35
2373.	2230.	13.	35.	1.30817×10^{-8}	2322.28	49.23	1.48	25.15	2087.41	117.44	631.53
2373.	2254.	13.	35.	1.50558×10^{-8}	2328.26	43.45	1.28	29.41	2120.91	103.68	738.50
2300.	2000.	13.	33.	5.79330×10^{-9}	2207.14	89.62	3.25	9.62	1773.63	216.75	238.73
2300.	2000.	13.	37.	6.41698×10^{-9}	2200.84	96.00	3.15	10.36	1778.44	211.20	263.07

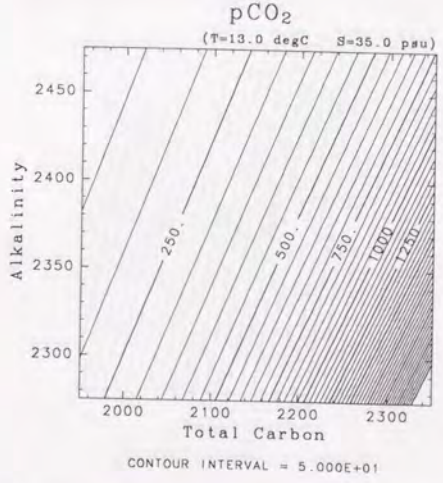

Figure A-1: pCO_2(μatm) at global temperature (13℃) and salinity (35psu).

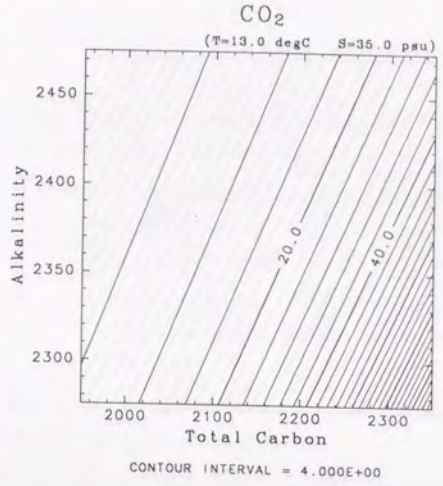

Figure A-2: CO_2concentration (μmol/kg) at global temperature (13°C) and salinity (35psu).

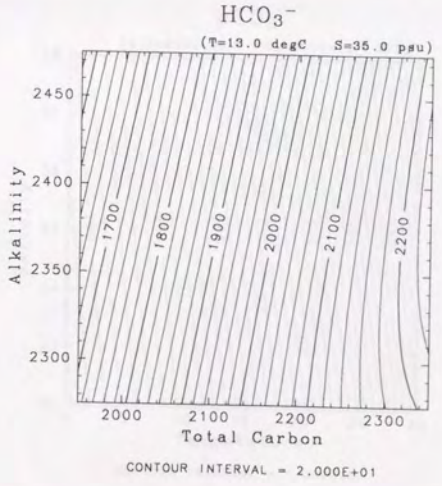

Figure A-3: HCO_3^-concentration (μmol/kg) at global temperature (13°C) and salinity (35psu).

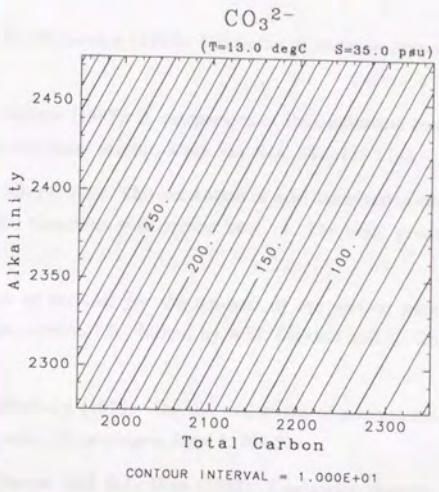

Figure A-4: CO_3^{2-}concentration (μmol/kg) at global temperature (13℃) and salinity (35psu).

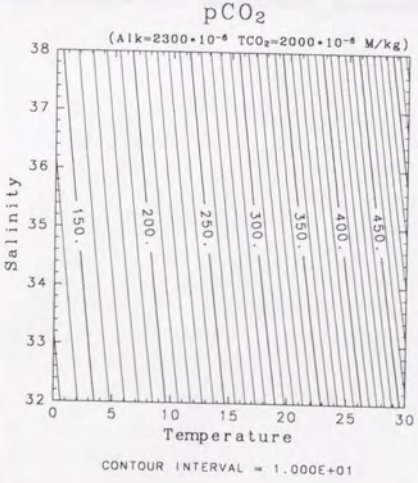

Figure A-5: $pCO_2(\mu atm)$ at $A_T = 2300\mu$mol/kg $\cdot$ $C_T = 2000\mu$mol/kg.

References

Culberson,C.H. and R.M. Pytkowicz (1973): Ionization of water in seawater., *Mar. Chem.*, 1, 403-417.

Dickson,A.G. and F.J. Millero (1987): A comparison of the quilibrium constants for the sissociation of carbonic asid in sea water media., *Deep Sea Res.*, 34, 1733-1743.

Dickson,A.G. and J.P. Riley (1979): The estimation of acid dissociation constants in seawater media from potentiometric titrations with strong base. I. The ionic product of water (K_w)., *Mar. Chem.*, 7, 89-99.

DOE (1991): *Handbook of methods for the analysis of the various parameters of carbon dioxide system in sea water*, version 1.0., Edited by A.G. Dickson and C. Goyet, U.S. Dep. of Energy, Washington, D.C..

Johansson,O. and M. Wedborg (1979): On the evaluation of potentiomatrictitrations of seawater with hydrochloric acid., *Oceanologica Acta*, 5, 209-218.

Takahashi,T., R.T. Williams, and D.L. Boss (1982): Carbonate chemistry. In:*GEOSECS Pacific Expedition*, vol3. Hydrographic Data,., 1973-1974. Edited by W.S. Broecker, D.W. Spencer and H. Craig, US Government Printing Office, 78-82.

Weiss, R.F. (1974): Carbon dioxide in water and seawater: the solubility of non-ideal gas., *Mar. Chem.*, 2, 203-215.

Appendix B

Dependence of Chemical Tracer Distributions on Vertical diffusion coefficient

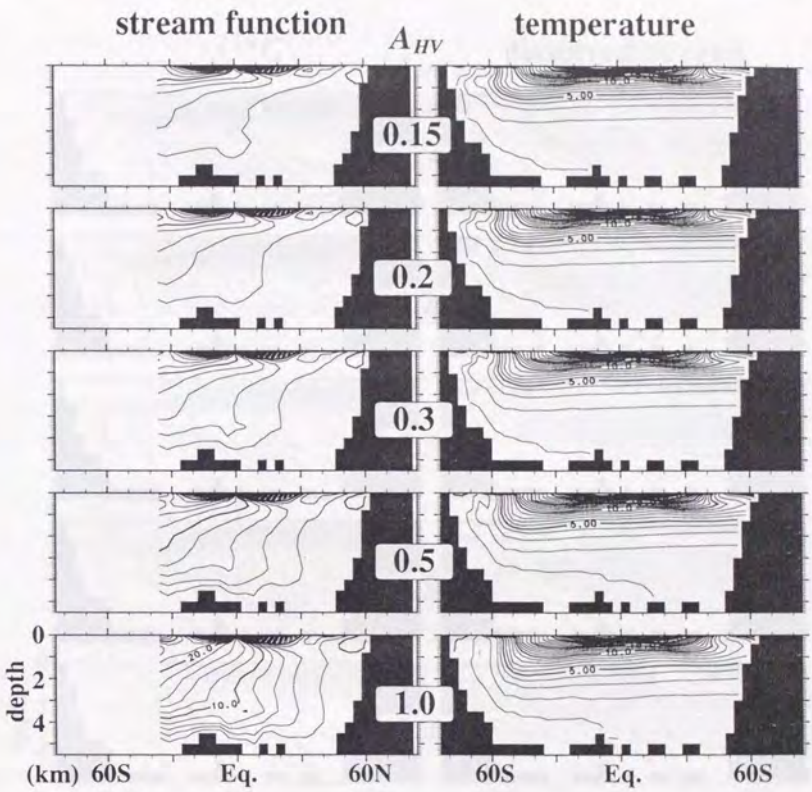

Figure B-1: Dependence of stream function (left-hand side, contour interval is 2Sv, 1Sv=$10^6 m^3$/sec) and temperature (right-hand side, contour interval is 1°C) in the Pacific on the vertical diffusion coefficient. The vertical diffusion coefficient is 0.15, 0.2, 0.3, 0.5, and $1.0\times10^{-4} m^2/s$ from the top panel to the bottom.

B.1 Dependence on vertical diffusion coefficient

Strength of thermohaline circulation is dependent on affects of vertical diffusion coefficient A_{HV} [Bryan, 1987]. Since the exchange rate between the surface and deep water affects the distribution of the chemical tracers, it is important to adopt an appropriate value for the coefficient of vertical diffusion A_{HV}. Before we calculate the distribution of the chemical tracers by using the biogeochemical general circulation model, we run the following five cases: A_{HV} =0.15, 0.2, 0.3, 0.5, and $1.0\times10^{-4} m^2/s$. We select the appropriate value for A_{HV} among these cases,

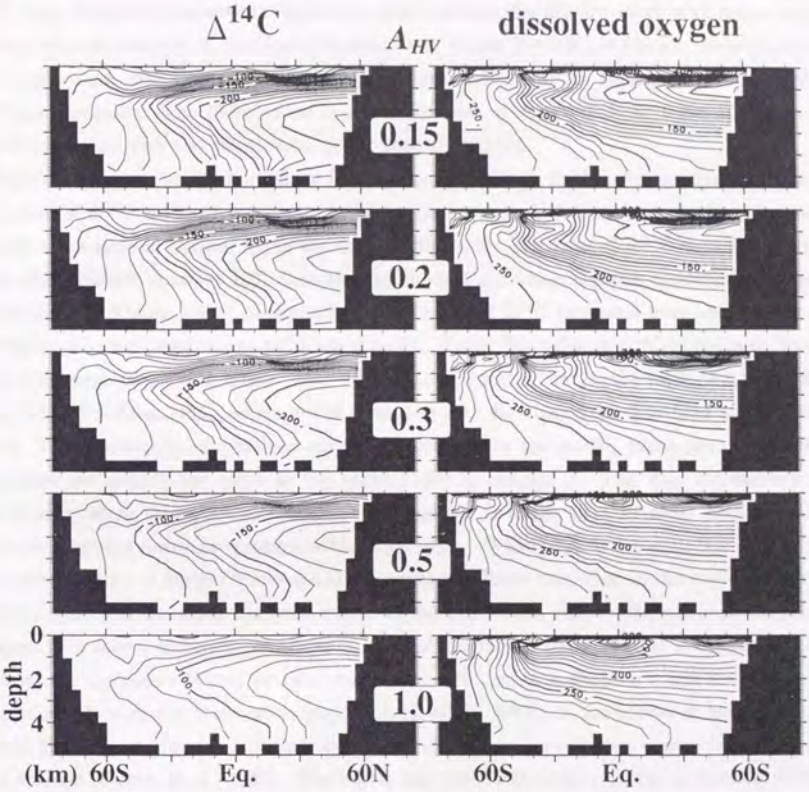

Figure B-2: Dependence of $\Delta^{14}C$ (left-hand side, contour intervals = 10‰) and dissolved oxygen (right-hand side, contour intervals = 20μmol/kg) in the Pacific on the vertical diffusion coefficient. The vertical diffusion coefficient is 0.15, 0.2, 0.3, 0.5, and $1.0\times10^{-4}m^2/s$ from the top to the bottom panel.

from the following discussion, especially the value of $\Delta^{14}C$ in the deep North Pacific.

Figure B-1 shows the meridional mass transport and the distribution of temperature in the Pacific meridional section. The mass transport is strongly dependent on A_{HV}: the inflow below the depth of 2km in the Pacific is from 5Sv for A_{HV} = 0.15 to 20Sv for A_{HV} = 1.0. The Ekman circulation, which is limited to the layer above the depth of 500m, is not dependent on A_{HV} as this meridional circulation is driven by wind stresses. The thermocline depth increases with an increase in A_{HV}. The temperature in the deep layer (about 1~3km) becomes higher

with A_{HV}. However, temperature below the depth of 4km slightly decreases with larger A_{HV}. This is because influence of the North Atlantic Deep Water (NADW) on the Pacific deep water becomes weaker with larger A_{HV}, and that of the colder Antarctic Bottom Water (AABW) becomes dominant. The thermocline depth in the case of $A_{HV} = 0.15$ or $0.2 \times 10^{-4}\mathrm{m}^2/\mathrm{s}$ is better compared with the observation better than the others.

Figure B-2 shows the distributions of δ^{14}C and temperature in the Pacific meridional sections. The value of Δ^{14}C in Figure B-2 is calculated by the method which includes biological processes (which is the same in chapter 3). In the deep North Pacific, the value of Δ^{14}C obtained by this method is younger of about 10‰ than that by the method which neglects biological processes (compare with Figure 2-9(b) in chapter 2). The error of Δ^{14}C produced from uncertainty of biological processes is estimated to be less than 5‰, if any. The value of Δ^{14}C in the deep North Pacific becomes larger with larger A_{HV}. When $A_{HV} = 0.2 \times 10^{-4}\mathrm{m}^2/\mathrm{s}$, the value of Δ^{14}C in the deep North Pacific is 240‰, which is well compared with the observation [Ostlund and Stuiver, 1980]. The distribution of dissolved oxygen is calculated in the model, whose parameters and constants are exactly the same as the control case in chapter 3. The A_{HV} dependency of the concentration of oxygen minimum at the equator is larger than in other regions. The nutrient trapping becomes stronger with larger A_{HV}. When A_{HV} is 0.5 or $1.0 \times 10^{-4}\mathrm{m}^2/\mathrm{s}$, the concentration of oxygen minimum at the equator is lower than that in the northern North Pacific. This feature is not changed, whatever the production rate r (defined in section 2 of chapter 2) is taken, although the absolute value of the oxygen concentration is changed.

From the discussion above, we take $A_{HV} = 0.2 \times 10^{-4}\mathrm{m}^2/\mathrm{s}$ in chapter 2 and 3. This value is comparable with the observation [e.g., Ledwell et al., 1993]. In the model of Maier-Reimer [1993], the vertical diffusion is mainly due to the computational diffusion caused by the advection scheme [Heinze *et al.*, 1992]. The inflow into the Pacific below 1.5km is 14Sv in Maier-Reimer [1993], which corresponds to our case of$A_{HV} = 0.5 \times 10^{-4}\mathrm{m}^2/\mathrm{s}$. Although his treatment of POC is different from ours, the minimum of dissolved oxygen concentration at equator is the common feature.

References

Heinze, C., E. Maier-Reimer, and K. Winn (1991): Glacial pCO_2 reduction by the World Ocean: Experiments with the Hamburg carbon cycle model., *Paleoceanogr.*, 6, 395-430.

Ledwell, J.R., A.J. Watson, and C.S. Law (1993): Evidence for slow mixing across the pycnocline

form an open-ocean tracer-release experiment., *Nature*, 364, 701-703.

Maier-Reimer, E. (1993): Geochemical cycles in an ocean general circulation model. preindustrial tracer distributions., *Global Biogeochem. Cycles*, 7, 645-677.

Ostlund, H.G., and M. Stuiver (1980): GEOSECS Pacific radiocarbon., *Radiocarbon*, 22, 25-53.

Appendix C

Phosphate Budget

C.1 Phosphate Budget

C.1.1 Boxes Analyzing Phosphate Budget

What is the dominant mechanism for determining the distribution of nutrients such as phosphate? For understanding of this mechanism, we estimate phosphate fluxes in the control case of chapter 2 between the boxes that represent an ocean divided into 5 levels in the vertical and 11 regions horizontally along the Broecker's "conveyor belt" [e.g., Broecker and Peng, 1982]. For simplicity, the Indian is not discussed here. The phosphate flux consists of four components: (1) horizontal flux due to advection and diffusion, (2) vertical flux due to advection and diffusion, (3) vertical POC flux, and (4) vertical flux due to convective adjustment.

C.1.2 Horizontal and Vertical Distribution of Phosphate Concentration

Phosphate flux due to POC settling decreases with an increase in depth as shown in Figure C-1(a). This flux is comparable with the other fluxes at 400m but is order of magnitude smaller at 3500m. In the euphotic layer (>50m in this figure), the export productions are maintained by upwelling in the equatorial region, and by convection at high latitudes. The horizontal distribution of phosphate at the depth of 500m is shown in Figure C-2(a), which is well compared with the observation [Levitus *et al.*, 1993]. The concentration of phosphate is high in the equatorial Pacific and the northern North Pacific, but is low in the subtropical gyre such as that in the North Pacific. The regions of high phosphate concentration correspond to these of high export production. As shown in Figure C-1(a), POC flux and vertical advective-diffusive flux are basically balanced in the upper thermocline (above 500m). This means that the phosphate concentration in a water below the area of high export production should be high. Upwelling of this water supplies phosphate to the euphotic layer, and as a result, the export production is maintained in these areas to be much higher than that in the other areas. This is the positive feedback mechanism called the nutrient trapping by Najjar *et al.*[1992].

Figure C-2(b) shows the horizontal distribution of phosphate at the depth of 925m, which is also weak compared with the observation [Levitus *et al.*, 1993] except that the model result for the Gulf of Guinea has a much higher value. Below the thermocline, high concentration of phosphate does not correspond to high export production, but corresponds to the old age of water mass. The concentration of phosphate in the deep water increases monotonically with an increase in the age of water from the North Atlantic to the North Pacific (this relationship has been widely used for determining abyssal circulation for a long time in oceanography). The reason is as follows: because POC flux is small and the horizontal advective-diffusive flux is

dominant in the deep layer (see Figure C-1(a)), the nutrient trapping dose not work at these depths. Water mass becomes gradually rich in phosphate with remineralization of POC during the advection from the North Atlantic to the North Pacific.

Figure C-1(b) and Figure C-3(b) show the pattern of the mass transport and its schematic diagram. There is a deep circulation from the North Atlantic to the North Pacific with upwelling of water to the surface, which is the conveyor belt of Broecker. The pattern of phosphate cycling may be different from the conveyer belt. Figure C-3(a) shows the schematic phosphate flux which is simplified from the phosphate budgets as shown in Figure C-1(a)). We found following two cycling systems of phosphate in the deep water which are almost independent of each other: one is in the Atlantic and the Southern oceans and the other is in the Pacific. We call them the Atlantic-Southern Nutrient Cycling System (ANCS) and Pacific Nutrient Cycling System (PNCS), respectively. In the deep Atlantic, the advective phosphate flux in the ANCS is dominant, and hence the pattern of phosphate cycling is similar to mass transport of NADW and AAIW (compare Fig.C-3(a) with Fig.C-3(b)). On the other hand, in the deep Pacific, the advective-diffusive flux in the PNCS is much weaker than that in the ANCS, but the POC flux is much stronger. Therefore, the phosphate cycling in the Pacific is quite different from the conveyor belt.

The high export production in the equatorial Pacific causes the following several features of the phosphate cycling in the PNCS. First, most of POC is usually remineralized at depths above the thermocline, but in the equatorial Pacific, a large quantity of POC is remineralized in the deep water because of the highest export production there. Upwelling of this phosphate-rich water supplies phosphate to the euphotic layer not only in the equatorial Pacific and but also in the North Pacific. This leads to the high export production in these regions (this is the effect of the nutrient trapping). Second, the phosphate maximum in the North Pacific is maintained not only by the *in situ* remineralization of POC, but also by the upwelling of the water rich in phosphate which is remineralized in the deep equatorial Pacific. Last, in the South Pacific, the horizontal advective-diffusive flux of phosphate is very small. This is because the horizontal advection flux from the Southern Ocean to the Pacific as a part of the conveyor belt is canceled out by the horizontal diffusion flux due to high concentration of phosphate in the deep equatorial Pacific. As mentioned above, the high productive regions such as the equatorial Pacific will cause the "apparent" closed circulation system of phosphate on the ocean scale, which is compared with the circulation of the conveyor belt on the global scale. This may be called another nutrient trapping ("ocean-scale nutrient trapping"), which should be separated from the original, "local nutrient trapping", proposed by Najjar *et al.*[1992].

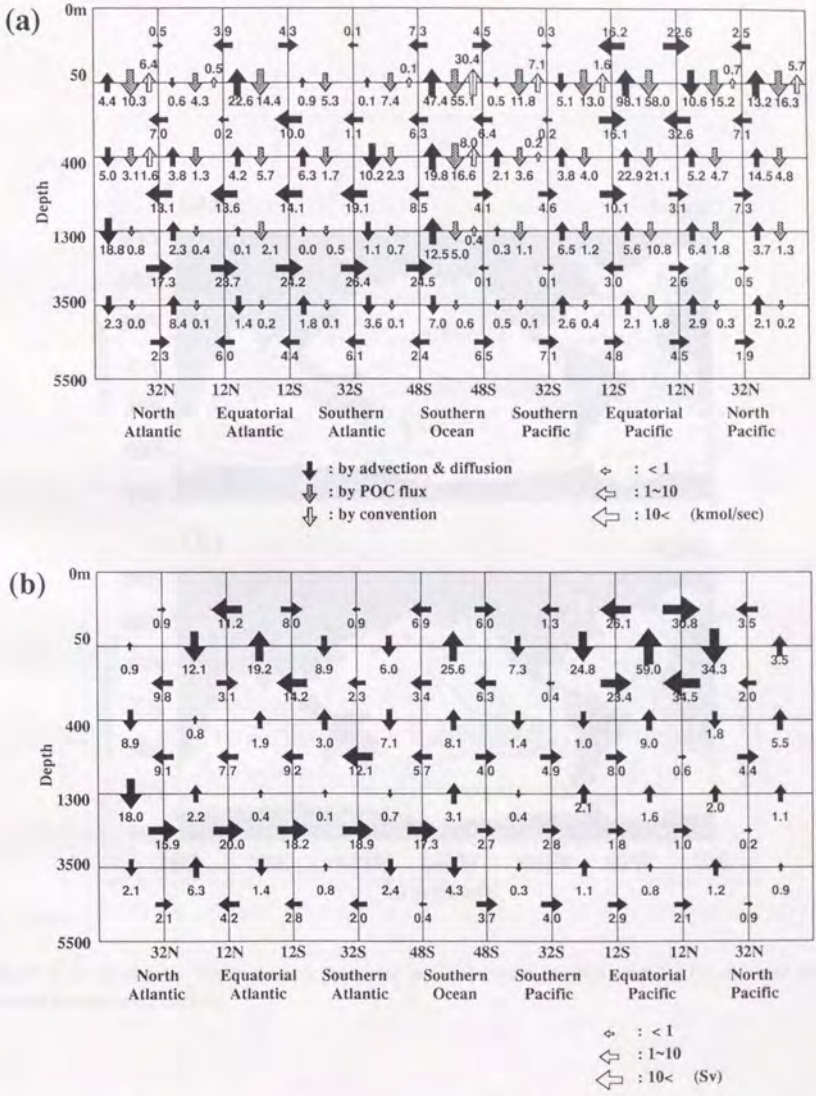

Figure C-1: Mass budget of water (a) and phosphate budget (b) along the Broecker's conveyer belt.

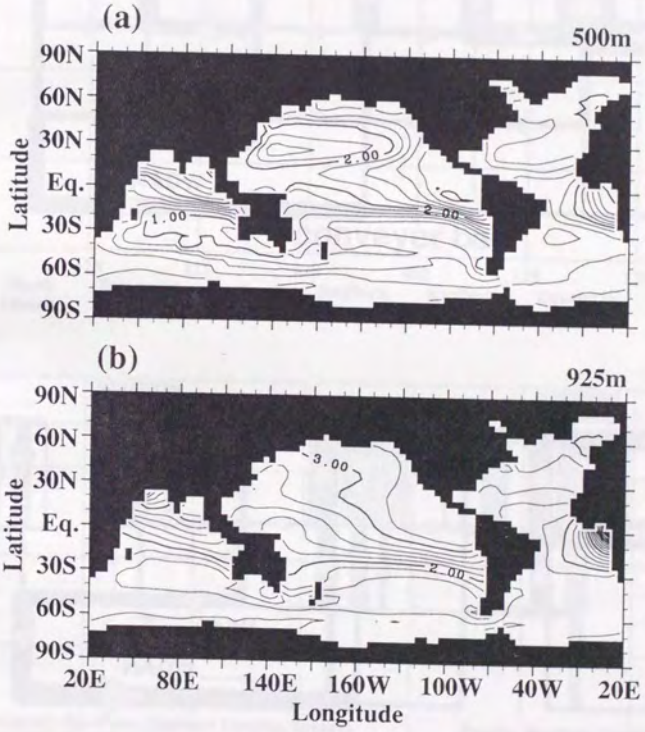

Figure C-2: Horizontal distributions of phosphate at (a) the depth of 500m, and (b) the depth of 925m. Contour interval is 0.2μmol/kg.

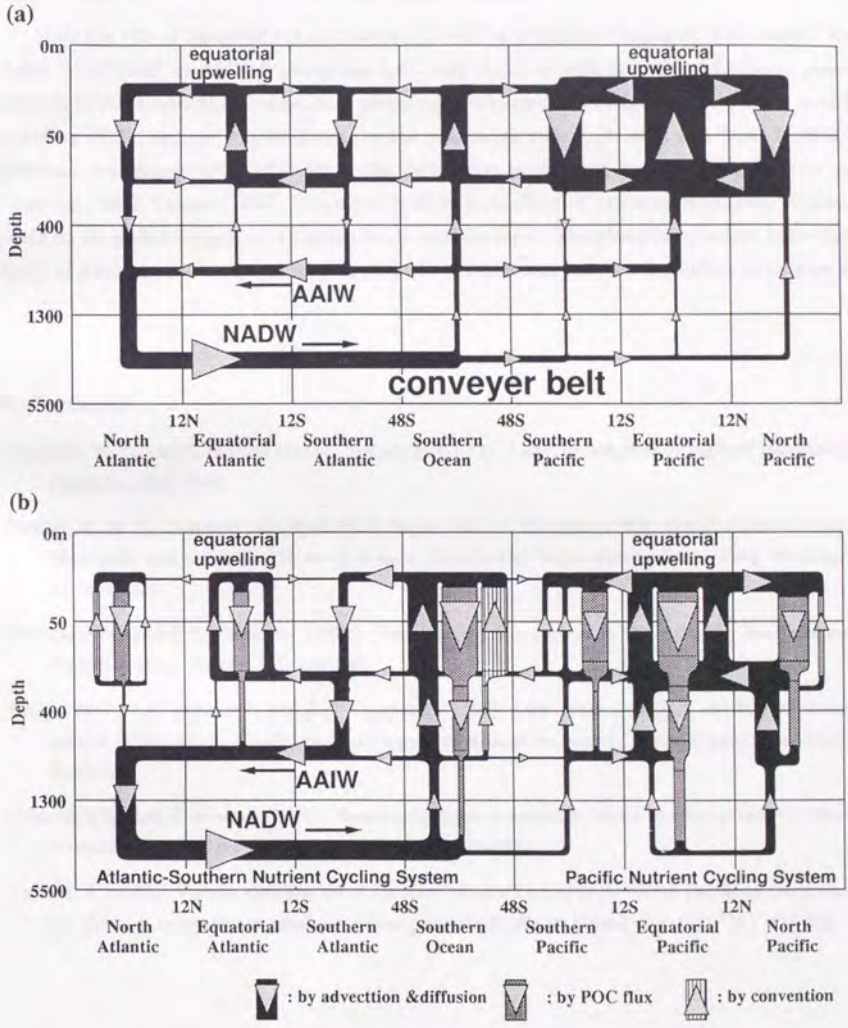

Figure C-3: Schematic diagram of mass transport (a) and phosphate cycling (b) along the Broecker's conveyer belt. It is noted that phosphate cycling in the Atlantic-Southern oceans and in the Pacific seems to be apparently closed systems.

C.1.3 The Effect of DOC on the phosphate budget

Here the role of dissolved organic matter (DOM) in phosphate transport is discussed. As Najjar *et al.*[1992] mentioned, phosphate transport balances with transport of organic phosphate in DOM. Horizontal divergence of phosphate integrated vertically is not zero in the model including DOM, and can not be ignored in the phosphate budget [Rintoul and Wunsch, 1991]. However, the concentration of DOM in the deep water is observed to be uniform [Martin an Fitzwater, 1992; Tanoue, 1992]. Therefore, if there is an effect of non-zero divergence of phosphate on its global budget, it is limited to the surface layer. The phosphate budget below the depth of 300m does not change even when DOM is taken into account as studied in chapter 3.

References

Broecker, W.S., and P.-H. Peng (1982): *Tracers in the Sea.*, Lamont-Doherty Geological Observatory, Palisades, New York.

Levitus, S., M.E. Conktight, J.L. Reid, R.G. Najjar, and A. Mantyla (1993): Distribution of nitrate, phosphate and silicate in the world oceans preindustrial tracer distributions., *Prog. Oceanogr.*, 31, 2445-273.

Martin, J.H., and S.E. Fitzwater (1992): Dissolved organic carbon in the Atlantic, Southern and Pacific oceans., *Nature*, 356, 699-700.

Najjar, R.G., J.L. Sarmiento, and J.R. Toggweiler (1992): Downward transport and fate of organic matter in the ocean: Simulations with a general circulation model., *Global Biogeochem. Cycles*, 6, 45-76.

Rintoul, S.R., and C. Wunsch (1991): Mass heat oxygen and nutrient fluxes and budgets in the North Atlantic Ocean., *Deep Sea Res.*, 38, Suppl. 1, S355-S377.

Tanoue, E. (1992): Vertical distribution of dissolved organic carbon in the North Pacific as determined by the high-temperature catalytic oxidation method., *Earth Planet. Sci. Lett.*, 111, 201-216.

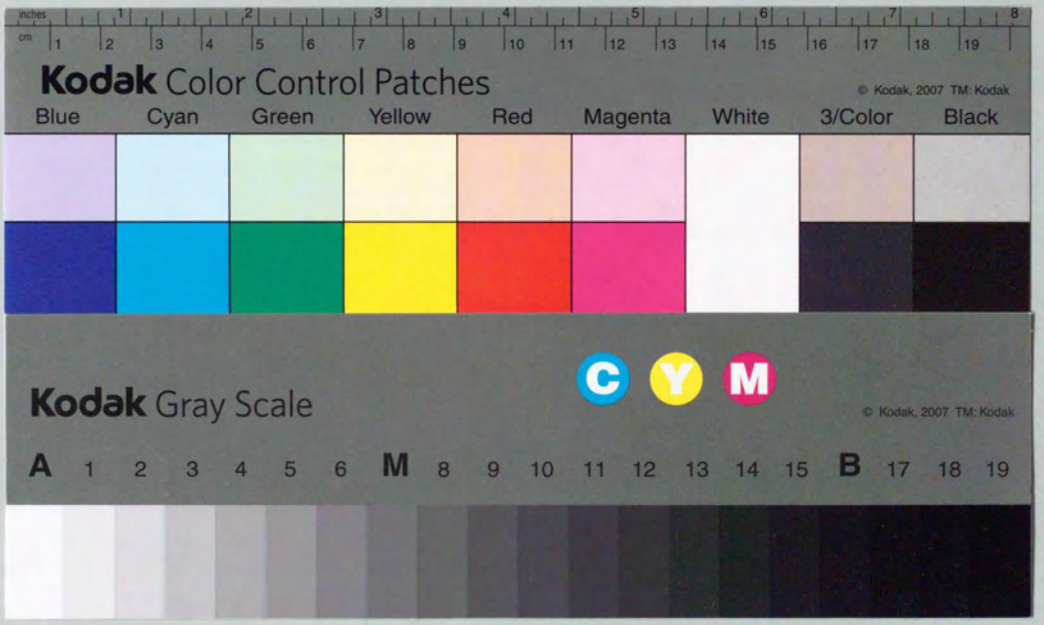
inches
cm
Kodak Color Control Patches
© Kodak, 2007 TM: Kodak
Blue
Cyan
Green
Yellow
Red
Magenta
White
3/Color
Black
Kodak Gray Scale
C
Y
M
© Kodak, 2007 TM: Kodak
A 1 2 3 4 5 6 M 8 9 10 11 12 13 14 15 B 17 18 19